HOCHSCHULE
KONSTANZ
TECHNIK, WIRTSCHAFT
UND GESTALTUNG

IOS
INSTITUTE FOR OPTICAL SYSTEMS


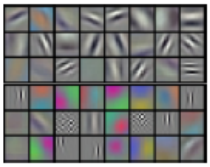

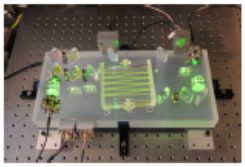
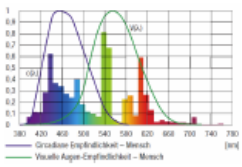

institute for optical systems
annual report 2015

Foreword

Hochschule Konstanz University of Applied Sciences (HTWG) has been one of the first Universities of Applied Sciences that has clearly committed itself to applied research. Today, HTWG has positioned itself in the growing group of research active Universities of Applied Sciences, and is continuously striving for even greater excellence, visibility, and leadership.

The research institutes play an essential role in the overall research activities of HTWG. The Institute for Optical Systems (IOS) has been founded as one of three focus institutes in 2008, and has lived up to its mission and HTWG's expectation ever since.

Measuring the success of research is generally a difficult task. It becomes easy, however, for individuals and institutes alike that contribute to the scientific community in many different ways. The IOS clearly is such an institute. Its members have published their work in numerous high quality publications, they have acquired substantial amounts of external funding, and they have successfully led several doctoral candidates to their advanced degree, to name only the most obvious contributions. The institute's success has only been possible because of the enthusiasm of its members, and its tight integration with HTWG. Students have contributed to the research work on various levels, and the results have been fed into the members' teaching. In this sense, the IOS has demonstrated the importance of excellent applied research also as a means for high quality teaching, in particular on the graduate level.

I am proud to write these few lines of thanks and congratulations for the IOS and cordially wish the institute, but first and foremost its members, ongoing enthusiasm, thirst for knowledge, and success for the future.

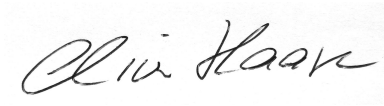

Prof. Dr. Oliver Haase
Vice-President for Research, University of Applied Sciences Konstanz

Preface

The present report gives an overview over the research and development activities of the Institute for Optical Systems (IOS) Konstanz in the year 2014. Our main fields of interest are cognitive systems, geometric modelling, image processing, optical metrology and light engineering, thus representing the fundamental disciplines of current optical technology. The focus on optical systems as a whole allows us to offer competent partnership to the local industry in all relevant aspects. The IOS was founded in April 2008 by four professors from three different faculties of the University of Applied Sciences at Konstanz and is led by Prof. Dr. Umlauf (director) and Prof. Dr. Franz (associate director).

The following project descriptions present ongoing activities mainly on a status report level. Most of the reports are written by students working on their diploma, bachelor, master or Ph.D. theses. They reflect the largely varying levels of content, practice and insight that are characteristic for an institution involved in academic education. Due to its interdisciplinary nature, research at the IOS combines approaches from optics, computer graphics, image and signal processing, metrology, light engineering and sensor technology typically resulting in optical systems on a prototype level, either in pre-phase research or in cooperation with local industry.

On the occasion of our annual report, we would like to thank all of our students and co-workers for their enthusiasm and dedication which makes our institute a great place to be. Special thanks go to our institute officers, Pascal Laube and Michael Grunwald, and to Jürgen Keppler for smoothly managing our day-to-day activities. We are also indebted to the administration and staff of the HTWG Konstanz for their help, especially president Dr. Carsten Manz and Prof. Dr. Oliver Haase, for their support and for continuing the start-up funding, and the faculties of Mechanical Engineering, Electrical and Information Engineering, and Computer Science with the deans Prof. Dr. Thomas Böttcher, Prof. Dr. Thomas Birkhölzer and Prof. Dr. Jürgen Neuschwander for their assistance. Furthermore we appreciate the support of the Institute for Applied Research (IAF) Konstanz, especially Prof. Dr. Horst Werkle and Dipl.-Ing. FH Andreas Burger.

Contents

Institute Profile

Institute for Optical Systems

Brauneggerstraße 55
Building E
3rd and 4th floor
78462 Konstanz

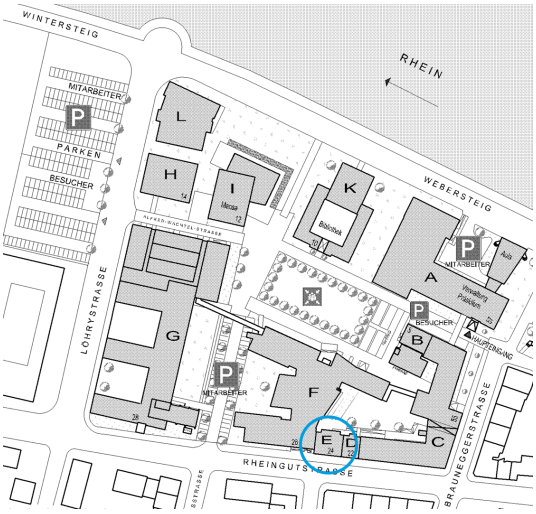

Location Plan

Prof. Dr. Georg Umlauf:

Diploma in computer science from University of Karlsruhe, 1996. Doctoral degree in computer science from University of Karlsruhe, 1999. PostDoc at University of Karlsruhe and University of Florida, Gainesville, USA, 1999-2000. Software development and senior researcher at Tebis AG, Hamburg, 2000-2002. Assistant professor for geometric algorithms at University of Kaiserslautern, 2002-2009. Interim professor for computer graphics at University of Karlsruhe, 2009. Since 2009 professor for computer graphics at University of Applied Sciences Konstanz and head of the computer graphics lab. Since 2010 member of the 'Institute for Optical Systems (IOS)' and 'Institute for Applied Research (IAF)'. Main research interests: Computer graphics, geometric modeling (splines, subdivision), reverse engineering, physical simulations.

Prof. Dr. Matthias Franz:

M.Sc. in Atmospheric Sciences from SUNY at Stony Brook, Diploma in physics from the Eberhard-Karls-Universität, Tübingen and doctoral degree in 1998. Thesis research in visual insect and robot navigation at the MPI for Biological Cybernetics and as a PostDoc at the Australian National University in Canberra. In industry he worked on various aspects of autonomous vision systems. 2002, he returned to the MPI as a group leader in the area of machine learning and computer vision. Since 2007 professor at the University of Applied Sciences in Konstanz and head of cognitive systems lab. Member of 'Institut für Angewandte Forschung (IAF)'. Main research activities in the development of automatically generated vision systems, optimisation and probabilistic modeling, with applications in industrial machine vision, texture analysis and steganalysis.

Prof. Dr. Claus Braxmaier:

Diploma in precision engineering at University of Applied Sciences Furtwangen. Diploma in physics and doctoral degree at the University of Konstanz in the field of fundamental tests of physics. Post-Doc at University of Konstanz. At EADS Astrium GmbH, system responsible for scientific and Earth observation missions for ESA and head of group 'Mission Metrology'. 2005-2013 professor for physics and control theory at the University of Applied Sciences Konstanz. Since 2013 ZARM Deputy Executive Director, Director Space Technology, and department lead "System Enabling Technologies" at the DLR-Institute of Space Systems, Bremen. Main research: high resolution optical metrology for industrial and space applications, tests of fundamental physics.

Prof. Dr. Bernd Jödicke:

Study of physics at the University of Kalrsruhe. Doctoral degree at Technical University Hamburg and University Karlsruhe in the field of high frequency technology. After that, industrial work at ABB Baden, Switzerland, as executive director for R&D. Since 1992 professor for applied physics at University of Applied Sciences Konstanz. Member of 'Institute for Applied Research (IAF)', 'Institut für Naturwissenschaften und Mathematik (INM)', 'Institute for Optical Systems (IOS) Konstanz' and 'Deutsche Lichttechnische Gesellschaft'. Head of laboratory for light engineering at HTWG. Main research activities in color and light measurements and color camera systems.

Prof. Dr. Burkhard Lehner:

Diploma in computer science from University of Kaiserslautern, 2004. Doctoral degree in computer science from University of Kaiserslautern, 2008. Software development at Sirona Dental System GmbH, Bensheim, 2008-2013. Since 2013 professor for computer science at University of Applied Sciences Konstanz. Since 2014 member of the 'Institute for Optical Systems (IOS)'. Main interests: software development, computational geometry, optical 3D measurement (especially in dental CAD/CAM).

Prof. Dr. Klaus-Dieter Durst:

Study of physics at the University of Stuttgart, 1986 doctoral degree in the field of magnetism at the Max-Planck-Institute of metal research. Thereafter research center Weissach of the Dr. Ing. h.c. F. Porsche AG, responsible for the central unit 'measurement technologies'. Since 1993 professor for measurement engineering and sensor technology at the University of Applied Sciences Konstanz. Member of 'Institut für Naturwissenschaften und Mathematik' and 'Institute for Optical Systems' Konstanz. Head of laboratories for measurement and sensor technology and production metrology. Currently director of 'Institut für Naturwissenschaften und Mathematik' Konstanz. Activities in the accreditation and surveillance of testing laboratories and inspection bodies.

IOS Staff

Professors	Georg Umlauf, director IOS Matthias Franz, associate director IOS Claus Braxmaier Bernd Jödicke Burkhard Lehner Klaus-Dieter Durst
Officer	Pascal Laube
Academic Staff	Leonard Thießen Markus Oswald Markus Meßmer Johannes Stühler Marco Fehrenbach Jens Müller Manuel Caputo Daniel Scherz
Postdoc	Thilo Schuldt
PhD Students	Michael Grunwald Martin Schall Pascal Laube Klaus Denker Jürgen Keppler Roman Byshko Dang Le Ruven Spannagel
Student Assistants	Martin Miller Korkiat Khumphai

External Fundings and Grants

- Baumer Inspection GmbH, Konstanz: "Farbtexturen in der industriellen Oberflächeninspektion", contract research.
- Baumer Inspection GmbH, Konstanz: "Inline - Inspektionstechnologie zum Farbabgleich für den digitalen Dekordruck", contract research.
- Australian Research Council, Pattern recognition in animals and machines: using machine learning to reveal cues central to the identification of individuals, Discovery Projects Grant.
- BMBF-Grant "Forschung für die Produktion von morgen" 2015, Entwicklung einer innovativen Anlagentechnik zur automatisierten und laserbasierten Reparatur strukturierter Formeinsätze - ToolRep.

Cooperations with Research Institutions and Industry

Academic and Institutional Cooperations

- University of Queensland, Brisbane
- Humboldt-Universität zu Berlin
- ZARM (drop tower), Center of Applied Space Technology and Microgravity, Bremen
- DLR Institut für Raumfahrtsysteme Bremen
- University of Tübingen
- Max-Planck-Institute for Biological Cybernetics, Tübingen
- German Federal Office for Information Security (BSI), Bonn
- Universität Konstanz
- University of California, Davis
- Technische Universität Kaiserslautern
- University of Florida, Gainesville
- Grenoble Institute of Technology
- University of Strasbourg

Industry Cooperations

- Siemens Postal, Parcel & Airport Logistics GmbH, Konstanz
- Sirona GmbH, Bensheim
- EADS Astrium, Immenstaad
- Breuckmann GmbH, Meersburg
- Chromasens GmbH, Konstanz

- Baumer Inspection GmbH, Konstanz
- Procon-System GmbH, Thierstein
- Lightdesign-Solutions GmbH, Dresden
- Knotenpunkt, Wenzel Präzision GmbH, Balingen
- Tebis AG
- Liebherr Aerospace GmbH, Lindenberg
- NTT Data Deutschland GmbH
- Lacuna Solutions GmbH

Theses and Student Projects

PhD Theses

- Pham Hai Dang Le, Detection of Steganography in Images with Statistical Models, Konstanz, 2014.
- Klaus Denker, Acquisition and On-line Reconstruction of 3D Point Data from Hand-held Laser Scanners and Multi-camera Stereo-matching, TU Kaiserslautern, 2014.
- Bartolomiej Piotr Siwek, Discrete methods for splines and subdivision curves, University of Oslo, 2015.

Master Theses

- Markus Friedrich , A parallel hash map for LOD-aware depth-map fusion, 2014.
- Michael Grunwald , Farbseparation im Tiefdruck, 2014.
- Martin Schall, Kamerakalibrierung mit Gaußschen Prozessen, 2014.
- Christian Gabele, Multioutput-Supportvektorregression, 2014.
- Marc Bumiller, Aufbau eines gegen die Aufnahmekonfiguration invarianten Klassifikationssystems, 2014.
- Christian Scheunemann, Entwicklung und Analyse geeigneter Bildmerkmale für die Verkehrszeichenerkennung anhand von synthetischen und realen Kamerabilddaten, 2014.
- Andreas Bug, Superresolution image reconstruction for barcode and optical character recognition applications, 2014.
- Rüdiger Schneider, Motivsuche in Proteinsequenzen, 2014.
- Merlin Blume, 3D Primitive Classification Using Stacked Autoencoders, 2015.

Bachelor Theses

- Simon Hein, Farbseparation, 2014.
- Steffen Holzhauer, Geometrische Kalibrierung mit Gaußschen Prozessen, 2014.
- Jonas Bublin, Vergleich und Bewertung von 3D-Rekonstruktion mit Commodity-Hardware, 2014.
- Leonard Thießen, Merging Multiple 3D Face Reconstructions, 2014.
- Patrick Roßnagel, Hand-held scanning of geometric primitives in virtual reality, 2014.
- Felix Peter, Optische Selbstlokalisation eines 3D-Druckkopfes im dreidimensionalen Raum, 2015.
- Tarek Schneider, VR-Scan-Simulation Raycasting von Spline-Flächen, 2015.
- Malvin Danhof, VR-Scan-Simulation Raycasting von Dreiecksnetzen, 2015.

Student Projects

- Marco Fehrenbach, Korkiat Khumphai, Felix Schuckert, On-line splat rendering, 2014.
- Mirko Indlekofer, Fabio Blaschke, VCam, 2014.
- David Simon, Dennis Bleicher, Jürgen Rieg, Point Cloud Label Tool, 2015.
- Simon Kesser, Tobias Keh, Felix Born, Surface Subdivision Tool, 2015.

Journal Papers

- Aguilera, D. N., H. Ahlers, B. Battelier, A. Bawamia, A. Bertoldi, R. Bondarescu, K. Bongs, P. Bouyer, C. Braxmaier, M.O.Franz, et al., "STE-QUEST ? Test of the universality of free fall using cold atom interferometry", Classical and Quantum Gravity, vol. 31, no. 11, pp. 115010, 2014.

- Schuldt, T., C. Schubert, M. Krutzik, L. Bote, N. Gaaloul, J. Hartwig, H. Ahlers, W. Herr, K. Posso-Trujillo, J. Rudolph, et al., "Design of a dual species atom interferometer for space", Experimental Astronomy, vol. 39, no. 2, pp. 167-206, 2015.

Conference Proceedings

- Thießen, L., P. Laube, M. O. Franz, and G. Umlauf, "Merging multiple 3d face reconstructions", Symposium on Information and Communication Systems, pp. 7-12, 2014.

- Caputo, M., K. Denker, M. O. Franz, P. Laube, and G. Umlauf, "Learning geometric primitives in point clouds", Symposium on Geometry Processing, Cardiff 2014, 2014.

- Denker, K., B. Hamann, and G. Umlauf, "On-line CAD Reconstruction with Accumulated Means of Local Geometric Properties", Curves and Surfaces, 8th International Conference, Paris 2014: Springer, pp. 181-201, 2015.

- Grunwald, M., J. Müller, M. Schall, P. Laube, G. Umlauf, and M. O. Franz, "Pixel-wise Hybrid Image Registration on Wood Decors", BW-CAR— SINCOM, pp. 24, 2015.

- Schall, M., M. Grunwald, G. Umlauf, and M. O. Franz, "Radiometric calibration of digital cameras using Gaussian processes", SPIE Optics+ Optoelectronics: International Society for Optics and Photonics, 2015.

- Danhof, M., T. Schneider, P. Laube, and G. Umlauf, "A Virtual-Reality 3d-Laser-Scan Simulation", BW-CAR— SINCOM, pp. 68, 2015.

Poster Presentations

- Caputo, M., K. Denker, M. O. Franz, P. Laube, and G. Umlauf, "Learning geometric primitives in point clouds", Symposium on Geometry Processing, Cardiff 2014, 2014.

Laboratories and Infrastrcture

The Institute for Optical Systems laboratories and infrastructure is composed of scientific equipment from the fields of Image Sensing, 2D and 3D Surface Analysis and Reconstruction as well as a powerful computing cluster for machine learning and high performance computing. Our laboratories and infrastructure is located in buildings *E*, *G* and *O* on the university campus.

The laboratory in building G includes equipment with focus on illumination engineering and high precicson stereoscopic surface scanning. The laboratory in buildig E comprises of camera callibration and spectrometric color measurement equipment, multispectral cameras as well as devices for 3D laserscanning, 3D visualization and 3D printing.

The computing cluster located in building *O* consists of GPU as well as CPU-Servers for high performance computing.

Most of the institutes workspaces are located on floors three and four of building *E*.

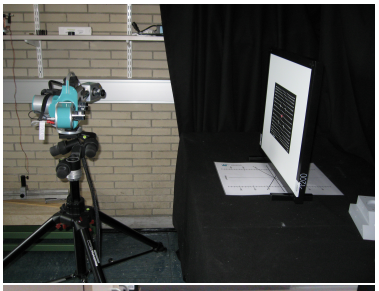

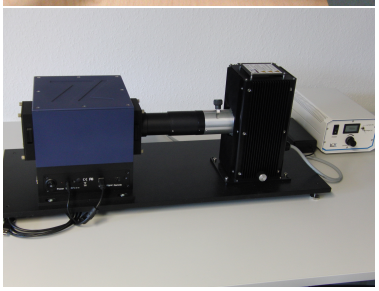

Research Activities

Calibration of digital cameras using Gaussian processes

Martin Schall, Michael Grunwald, Georg Umlauf and Matthias O. Franz

Digital cameras are subject to physical, electronic and optic effects that result in errors and noise in the image. These effects include for example a temperature depedent dark current, read noise, optical vignetting or different sensitivites of individual pixels. The task of radiometric calibration is to reduce these errors in the image and thus improve the quality of the overall application. We present an algorithm for radiometric calibration based on Gaussian Processes. Gaussian process regression is used to learn a temperature and exposure time dependent mapping from observed gray-scale values to true light intensities for each pixel. Runtime is reduced by partitioning pixels into groups and choosing one represenative pixel each while minimizing the quality reduction.

Introduction

Many scientific and industrial applications, e.g. astronomy or bioinformatics, depend on images that accurately represent the observed scene. Images taken from digital cameras with CCD or CMOS sensors are subject to a large variey of error sources. Most errors are created by the sensor noise which has four fundamental sources *photon* or *shot noise*, *Fano noise*, *fixed pattern noise* and *read noise*. These errors corrupt the measured gray-scale values of the image and are mostly dependent on the brightness of the observed scene, exposure time and sensor temperate while others are constant for any pixel.

Radiometric calibration quantifies these errors and noises. This is done individually for each camera setup in order to reduce influence on the images. Fixed pattern noise, varied sensitivites of individual pixel and vignetting can be reduced using radiometric calibration of the camera. Regression models can be used for radiometric calibration by estimating the correct intensities of the image pixels based on the observed intensities and known camera parameters. The used regression model approximates a function $f : \mathbb{R}^3 \to \mathbb{R}$ with the independent variables being the observed intensity of the pixel, exposure time and sensor temperature. The dependent variable is the correct intensity of the pixel.

Our work [**?**] is a machine learning approach that models arbitrary pixel characteristics dependent on exposure time and sensor temperature. The learning approach infers pixel characteristics from training examples. Gaussian processes is used for regression and is a machine learning method which can be used for extrapolation, regression and interpolation. Based on learned information, the Gaussian process can give a prediction for the relation of unseen data. Gaussian processes were chosen for regression because they adapt well to non-linear functions with added noise, as described by Rasmussen and Williams [**?**].

Current Status

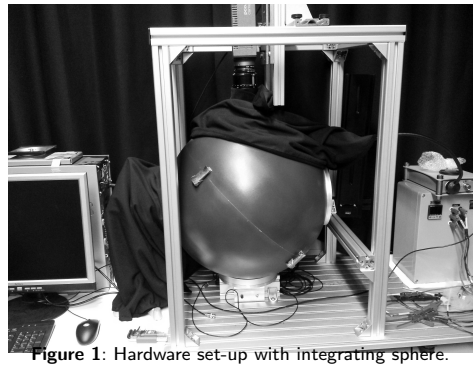

Figure 1: Hardware set-up with integrating sphere.

An important part for the work was creating training and evaluation data for the Gaussian processes. A hardware setup (shown in figure **??**) consisting of an integrating sphere, digital camera, LED light source and photometer has been set up in an optical laboratory at the HTWG Konstanz. An integrating sphere in combination with the LED light source is used as a controllable, homogenous light source. Light intensity within the integrating sphere is measured by the photometer as the reference value and noisy images are taken by the digital camera that will be calibrated. A total of 200 training images were taken, evenly spaced over the specified sensor temperature range, exposure time and light intensity. The camera parameters and measured light intensities

were stored together with the taken images to allow calculating the regression model from measured light intensities to true intensities.

Images were taken with a spatial resolution of $4008x2672$ pixels. Each pixel of the sensor is expected to show an individual characteristic and thus the optimal reconstruction quality can be achieved by calculating one regression model per pixel, taking the individual characteristic of each pixel into account. Since calculating a Gaussian process regression model is computationally costly, individual regression models per pixel are infeasible for high resolution images. On the other hand, calculating one regression model for the whole image would not accurately mode the individual pixel characteristics.

The chosen way to solve this is to partition the pixels of the camera sensor into partitions of equal size, each containing pixels with approximately the same characteristic. This can be done by sampling the pixel characteristics from a small number of images and lexical sorting of the pixels using the sampled characteristics as keys. In the sorted list of pixels, neighbouring ones show a identical or similar characteristic. This list is split into partitions of equal size. One pixel per partition is chosen as the representative pixel for which the regression model is calculated. In order to minimize the reconstruction error caused by partitioning, the pixel with the minimal Euclidean distance of its mean value and variance to the whole partition's mean and variance is selected as the representative pixel.

One regression model is calculated for each partitions representative pixel using the previously generated training images. Gaussian processes in function space using Gaussian radial basis functions as the covariance function are used for regression. This allows adaption to non-linear functions while prefering smooth regression functions. Radiometric calibration of the digital camera was done by estimating each pixels correct gray-value using the measured value and camera parameters as inputs for the regression function of the related representative pixel.

Using this algorithm, the runtime for calculating the regression models for a $4008x2672$ pixels image with 4000 partitions was reduced to 990 seconds using off-the-shelf hardware. Restoration of one image took 120 seconds. The mean squared error of the restored images was reduced from (depending on the use case) between 3.7% and 4.5% to between 3.1% and 3.6% of the MSE in original, uncalibrated images.

Future Work

The current implementation of this work shows that the quality of the radiometric calibration of digital cameras can be improved using regression models based on Gaussian processes. The necessary runtime for the reconstruction of one images does only allow offline applications, but no online use in industrial applications. Further research is necessary to speed up the algorithm or use more suited implementations, e.g. utilizing the GPU of the computer, for the implementation of the algorithm.

Bibliography

[1] Rasmussen, C. E. and Williams, C. K. I.: Gaussian Processes for Machine Learning (Adaptive Computation and Machine Learning), 2006.

[2] Schall, M., Grunwald, M., Umlauf G. and Franz, M. O.: Radiometric calibration of digital cameras using Gaussian processes, 2015.

Deep Learning methods in Convolutional Neural Networks

Matthias Hermann, Martin Schall and Matthias O. Franz

Research in Artificial Neural Networks has seen important improvements in shape of Deep Learning [**?**] and Deep Neural Networks in recent years. This effort lead for example to the first computer system capable of beating human masters in the game of Go [**?**]. We conducted broad research into the field of Deep Learning, especially Convolutional Neural Networks [**?**] to implement these methods and reproduce the reported results. This work provides a foundation for further research with Artificial Neural Networks and applying these to real-world problems at the Institute for Optical Systems.

Introduction

Artificial Neural Networks started out as mathematical models of biological neurons and neural networks in the 1950's. Since then they have been subject of many studies and research and have been developed into a machine learning method suitable for a wide range of tasks like classification, regression, object detection, feature extraction or handwriting recognition. They consistent of networks of artificial neurons, each providing only very basic mathematical function, but the combined network is capable of approximating highly non-linear functions [**?**]. Training of Artificial Neural Networks is done by applying a large data set with known in- and outputs, 'showing' one sample at a time to the network and correcting the error done at each sample. This so called supervised training using the backpropagation algorithm was first successfully applied to Deep Neural Networks in 2006 [**?**] and has since allowed a wide variety of research and applications in Deep Learning.

Convolution Neural Networks [**?**] are well suited for tasks with image (e.g. objects or textures) or geometric (e.g. point clouds) input. They allow the automatic end-to-end learning of low-level filters like edge detectors combined with high-level tasks like object classification. This makes them a research interest for a number of projects at the Institute for Optical Systems.

The presented work consists of a structured inquiry of state-of-the-art methods in Convolutional Neural Networks, as well as the implementation and evaluation of these methods. The work reproduced published results on public databases with the same or near same quality as documented in the publications.

Methods and findings

An implementation of Convolutional Neural Networks and related training algorithms has been done on basis of state-of-the-art publications in the field. It has been successfully applied to the MNIST handwritten digit database and CIFAR10 object database. CIFAR10 consists of images of ten different classes (e.g. dogs or airplanes) with the task of correctly classifying the image. Figure **??** shows the first layer of convolutional kernels of a network trained for this task. It shows an interesting observation with Convolutional Neural Networks: The first convolutional layer learns Gabor-like filter kernels that are also present in the early vision in nature. This is an example of Artificial Neural Networks imitating biological functionality without explicitly training the network to achieve this.

The end-to-end classification with a CNN is then performed by repeatedly applying convolutional kernels and feature extraction to the data. This allows to extract a few high-level features (the classification of each sample) from many low-level features (the image's pixels colors).

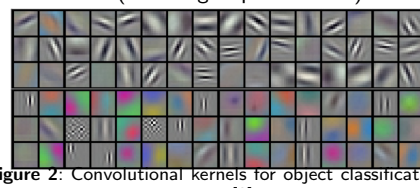

Figure 2: Convolutional kernels for object classification. Image by Alex Krizhevsky [**?**]

The presented work also includes the evaluation of improvements for Convolutional Neural Networks and their training methods:

- Optimization methods, e.g. Stochastic Gradient Descent, Nesterov Momentum, RMSProp, AdaDelta, Equilibrium SGD.

- Regularization methods: L1-, L2-regularization, early stopping and dropout learning.
- Max, average and stochastic pooling layers.
- Visualizations of Convolutional Neural Networks and their training process.

Classification-, regression- and autoencoder-tasks were tackled in the presented work. Figure **??** shows the convergence of training and validation error rates for MNIST - the task of classifying handwritten digits zero to nine - with different optimization methods. The topology, hyperparameters and initialization of the network itself was kept constant over all experiments. It shows that choosing a suitable optimization method is critical for speeding up the convergence rate and overall error rate. This is an observation that can be made for other aspects in Deep Learning as well: Good results can be achieved quickly with basic approaches, but correctly handling the details lead to the best results in the end.

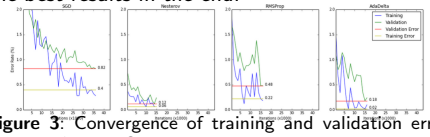

Figure 3: Convergence of training and validation error rates for MNIST

Next steps

The presented work successfully implemented and evaluated state-of-the art methods of Convolutional Neural Networks at the Institute for Optical Systems. This allows further research into this topic and the application of the gained knowledge to running and future projects. Of particular interest are applications in object detection, texture analysis and geometric reconstruction. Other successfully applications like playing the game of Go [**?**] at a master's level or recognizing the geolocation of vacation pictures [**?**] show that Convolutional Neural Networks can be applied to a wide variety of problems. This reinforces the research and application of a Deep Learning approach to more visual and geometric problems.

Bibliography

[1] J Schmidhuber. Deep Learning in Neural Networks: An Overview. Technical report, 2014.

[2] David Silver, Aja Huang, Chris J. Maddison, Arthur Guez, Laurent Sifre, George van den Driessche, Julian Schrittwieser, Ioannis Antonoglou, Veda Panneershelvam, Marc Lanctot, Sander Dieleman, Dominik Grewe, John Nham, Nal Kalchbrenner, Ilya Sutskever, Timothy Lillicrap, Madeleine Leach, Koray Kavukcuoglu, Thore Graepel, and Demis Hassabis. Mastering the game of Go with deep neural networks and tree search. *Nature*, 529(7587):484–489, 2016.

[3] Alex Krizhevsky, Ilya Sutskever, and Geoffrey E Hinton. ImageNet Classification with Deep Convolutional Neural Networks. *Advances In Neural Information Processing Systems*, pages 1–9, 2012.

[4] Vera Kurkova. Kolmogorov's theorem and multilayer neural networks. *Neural Networks*, 5:501–506, 1992.

[5] Geoffrey E Hinton, Simon Osindero, and Yee-Whye Teh. A Fast Learning Algorithm for Deep Belief Nets. *Neural Computation*, 18(7):1527–1554, 2006.

[6] Tobias Weyand, Ilya Kostrikov, and James Philbin. PlaNet - Photo Geolocation with Convolutional Neural Networks. Technical report, 2016.

Detection of flowmarks on laminated decor using texture features

M. O. Franz, H.-P. Diehl[1]

The production process of laminated decors is subject to a large variety of perturbations some of which are very hard to detect by machine vision algorithms. Among the most notorious are flowmarks that are caused by processing errors during lamination. Flowmarks are only visible in certain lighting and viewing conditions, and only show up with a very small texture contrast. In this project, we developed a new detection algorithm for flowmarks that is based on higher-order texture features in combination with support vector classifiers.

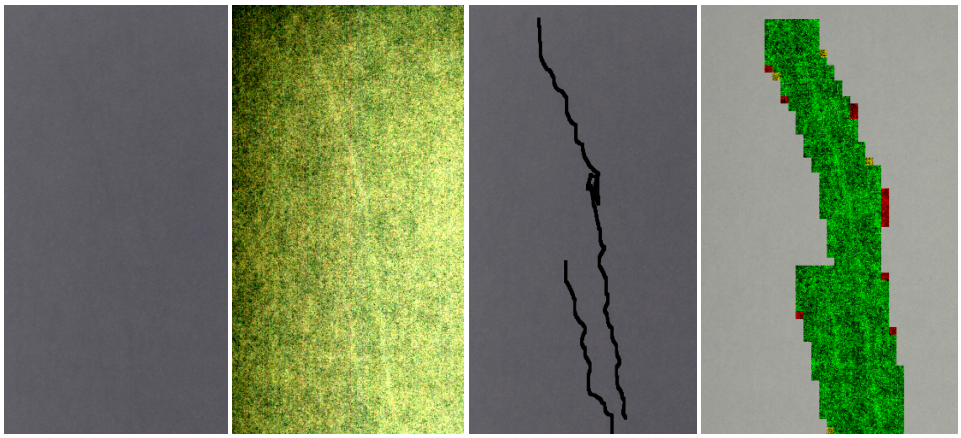

Figure 4: *Left:* Example of flowmarks on a laminated decor shown in the original contrast; *middle left:* Contrast maximized image of the flowmarks; *middle right:* Hand labeling for training and testing the detection system; *right:* detector output - detected regions that contain flowmarks are marked in green, erroneous detections in red.

Flowmarks usually appear as low-contrast linear structures that are very hard to detect in a textured background (see Fig. 1, left). However, to the human eye these structures are still visible under certain viewing angles and possibly disturbing. From the point of view of machine vision, flowmarks are particularly hard to detect as they show themselves only by small alignments of texture elements, not by different contrasts or colors. In terms of statistics, this means that flowmarks can only be detected by analyzing higher-order pixel dependencies, i.e. dependences between three or more pixels. We therefore used higher-order texture features that were previously only applied to problems in steganalysis[2]. For training our detector, we labelled flow marks by hand and subsequently divided the images in overlapping regions (see Fig. 1, middle right). The texture in each region was characterized by its higher-order features which comprised the input to a support vector machine. The training of the detector required about 5000 image regions before a satisfactory detection rate could be achieved. The trained detector has a very low false alarm rate while correctly marking the majority of all image regions contaminated by flowmarks (see Fig. 1, right).

[1]Baumer Inspection GmbH, Lohnerhofstrasse 6 78467 Konstanz

[2]Pevny, T., et al.: Steganalysis by subtractive pixel adjacency matrix. IEEE Trans. Info. Forensics and Security, 5(2), 215-224, 2010.

Precise Characterization of the Nonlinear Spatial Transfer Function of Monitors

M. O. Franz, U. Wannek[1], F. A. Wichmann[3]

Psychophysical experiments and technical applications (e.g. in radiology or remote sensing) often require displaying images with high fidelity on a monitor. In order to assess monitor quality, one needs to measure its spatial transfer function which characterizes the linear and nonlinear interactions of neighboring pixels. In the literature, there exists no established method for measuring the nonlinear aspects of the transfer function. Here, we propose a new nonlinear method based on implicit Volterra series which – for the first time – opens up the possibility of measuring such nonlinear pixel interactions.

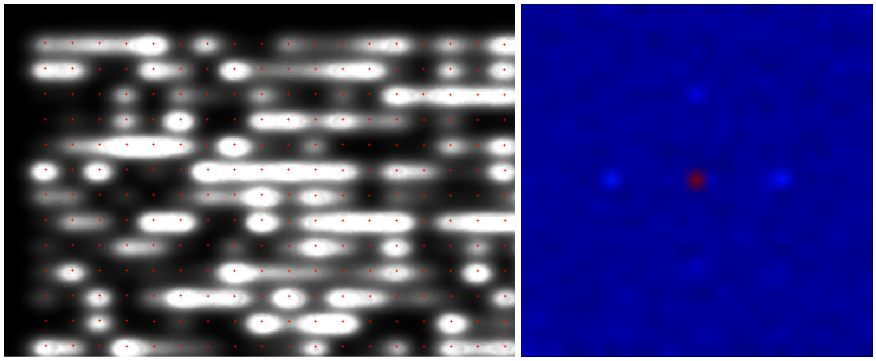

Figure 5: *Left:* Enlarged view of a CRT displaying a noise pattern. The lateral smearing of the pixels leads to strong interactions in the horizontal direction and an undesired damping of the displayed high spatial frequencies. The red dots indicate the pixel centers automatically detected by the image processing algorithm. *Right:* Second order Volterra kernel of the CRT monitor as measured by the new method. The small peaks (bright blue) around the central peak (red) indicate nonlinear interactions between neighboring pixels.

Volterra kernels are well suited for systematically characterizing linear and nonlinear interactions between neighboring monitor pixels. However, the traditional method for measuring these kernels by cross-correlation requires an excessive amount of test images which made the application of this method to measuring the spatial transfer function of monitors prohibitive. A recently developed method by one of the authors[4] estimates Volterra kernels using nonlinear polynomial kernel regression which vastly reduces the amount of required test images while achieving a much higher accuracy as compared to traditional cross-correlation. In this project, we applied the new estimation method for the first time to the spatial transfer functions of monitors.

The analysis was based on high-resolution images of the monitor surface taken with a calibrated luminance camera (see detail in Fig. 1, left). The pixel centers were automatically detected by a region counting algorithm applied to a binarized and morphologically processed version of the image. We extracted the image regions around the detected pixel centers and used them as the measured luminance output of the monitor for a given input image. This precise correspondence between input and output image allowed us to estimate the nonlinear transfer function in the form of a Volterra series. First measurements show that nonlinear pixel interactions do indeed play a role even in high quality monitors (see Fig. 1, right), thus leading to undesired nonlinear distortions in the displayed images.

[3]University of Tübingen, Dept. of Computer Science, Neural Information Processing, Sand 6, 72076 Tübingen

[4]Franz, M. O., and B. Schölkopf: A unifying view of Wiener and Volterra theory and polynomial kernel regression, *Neural Computation* 18(12), 3097–3118, 2006.

Modeling of Decisions in Reef Fish with Machine Learning

M. O. Franz, U. Siebeck*, A. Parker*, G. Wallis*

*School of Biomedical Sciences and School of Human Movement and Nutrition Sciences, The University of Queensland

Some reef fish are capable of visually recognizing thousands of different individuals although they do not dispose of any evolutionary advanced cortical structures in their brains. Often tiny differences in the facial patterns are the only visual cues available for this task, but it is still unknown which of these cues might play a role in the recognition process. In our study, we use machine learning models of the underlying decisions to identify these cues and to assess their relative importance.

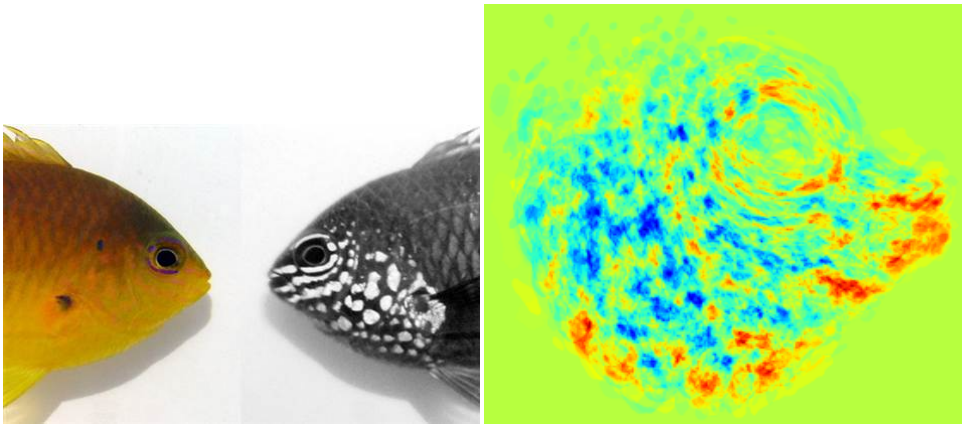

Figure 6: Left: Damselfish (appearance in the visual range is shown left) can distinguish between conspecifics by looking at the ultraviolet patterns on their faces (appearance in the UV range is shown right). Right: A color coded map of the relevance of each facial region for recognizing this fish species (decision image) obtained from machine learning. Green regions are irrelevant, red regions have a positive weight for the decision, blue regions a negative weight.

Superficially, fish might not appear to be the first choice for being studied by a neurobiologist as they do not possess any evolutionary advanced brain structures such as the cortex in the mammalian brain. But exactly this makes them interesting from a neurobiological point of view: although their brain structure might be comparatively simple, fish (and particularly reef fish) sometimes show astonishing cognitive capabilities. Cleaner fish, for instance, often discriminate between thousands of "customer" fish and adapt their cleaning behaviour to the individual needs and preferences of the customer. In humans and mammals, such behavior usually involves cortical brain structures, but fish achieve this by using a much more primitive neural architecture. This simplicity opens up the opportunity for neurobiology to understand higher cognitive functions by studying simple neural architectures.

The present project is a collaboration between neurobiologists of the University of Queensland, Australia, and the IOS Konstanz. We focus on the visual discrimination between certain species of reef fish which is based on complex facial patterns (visible in the ultraviolet range, see Fig. 1). The exact nature of the visual cues used for this task was still unknown at the onset of the project, so the goal was to identify these cues and assess their relative importance.

Figure 7: Laboratory environment for conducting fish experiments. The fish are captured in the wild and kept in individual tanks. They are trained to discriminate between various fish species by presenting them images and rewarding a correct choice.

To achieve this goal, we conducted a large number of behavioral experiments with captured reef fish in the laboratory of Dr. Siebeck. In each experimental trial, the fish was presented facial images from two different fish species (a target and a distractor species, see Figs. 2,3). When the fish swam to the target fish species it was supposed to learn, it received a reward. After training, the recognition performance of the fish was tested on new, previously unseen images to make sure it actually learnt the discrimination task. At the same time, we trained a learning machine on exactly the same image data to reproduce the behavioral decisions of the fish as closely as possible. In this way, the learning machine became a mathematical model of the underlying decision process of the fish.

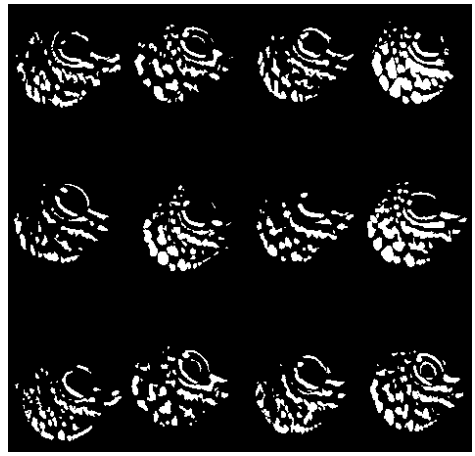

Figure 8: Binarized facial patterns used for training the fish and the learning machine in the experiments.

In contrast to the fish brain, the trained learning machine can be directly analyzed. We extracted so-called *decision images* which may be interpreted as a map that associates a weight to each image region (Fig. 1). The weight indicates the relevance of the image region for the decision process. Image regions which are important for discriminating the target fish species have a high positive weight, image regions which are important for recognizing the distractor species a high negative weight. The example in Fig. 1 shows that the modelled fish used the eye region and the lower part of the facial pattern for recognizing the target species.

LabelImage Tools

Sonja Futterknecht, Tobias Birkle, Benjamin Kugler, Robin Mattes and Michael Grunwald

Machine learning needs a lot of training data to detect objects in images. To generate the training data, we developed a software soultion to label and classify fishes in images. This project was in cooperation with the Global Change Institute of the University of Queensland.

Introduction

Regarding the number of fishes and their diversity it is possible to investigate the consequences of the climate change in coral reefs. This is the project of the Global Change Institute (GCI) at the University of Queensland under the head of Prof. Dr. Ove Hoegh-Guldberg. In order to specify the number of fishes experts dive through the coral reefs and document the fish population. Another project at the GCI is the *XL Catlin Seaview Survey*, in which coral reefs are photographed using underwater cameras, as shown in figure **??**. The images of the reefs are published on the website *globalreefrecord.org*. The *FishNet* project, under the management of Dr. Ulrike Siebeck from the GCI wants to use the underwater photos of the coral reefs from the *XL Catlin* project to identify fishes and their number in the images. To detect the fishes a software soultion will be developed using methods of machine learning. In the first step the fishes have to be labeled and classified in the photos manually to extract their features. For this part of the software solution a software called *LabelImage* is developed to label and classify the fishes. These labeled fishes are the training images for the machine learning. Based on the training images the features of the fishes will be learned and it will be able to find these features in not yet labeled images. The manual labeling and classification of the fishes will be done by the experts of the *FishNet* team.

Current Work

The software was developed with Python 3.4 and PyQt 5. With this application a rectangle can be drawn around the fishes with one mouse click to label and classify them (see fig. **??**). The coordinates of the labeled area and the corresponding fish species will be saved in an XML document. In a separate extraction module of the software the labeled fishes will be extracted from the original image with the help of the XML document. The extracted patches will be saved as single images. The patches can be used as training images for the machine learning. They form the basis for the automatic identification of the fishes. The determination of the species diversity and the number of the fishes works the better the more data is available for the software solution. To submit many fishes and thus training data to the soft-

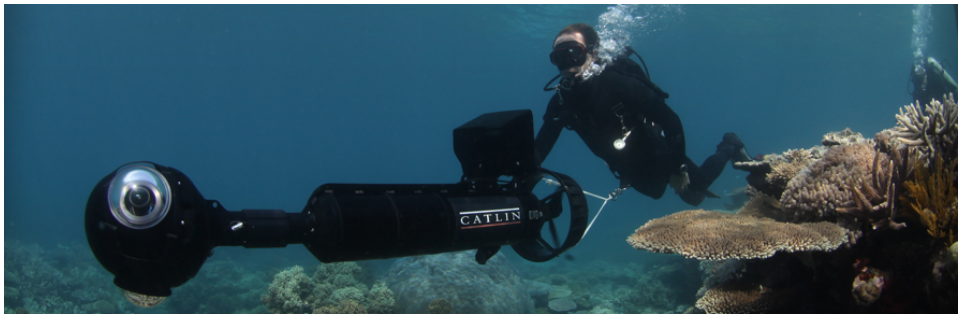

Figure 9: *XL Catlin Seaview Survey* expert diving through coral reef. (globalreefrecord.org)

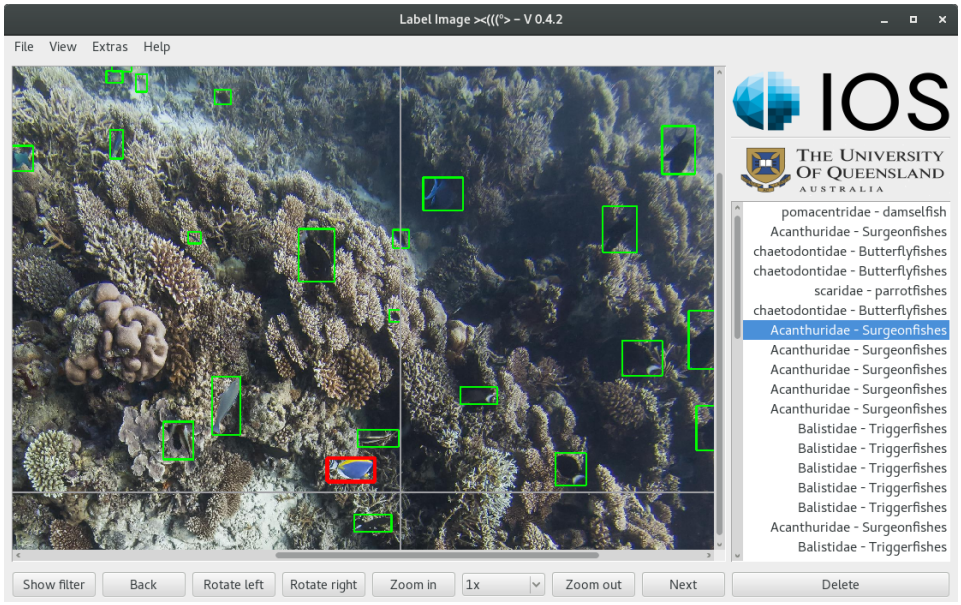

Figure 10: *LabelImage* software with labeled fishes.

ware solution the fishes are not only labeled by the scientists of the GCI but also by interested users. Therefore in the second part of the team project a web based software solution was developed using HTML5 and the JavaScript framework jQuery which allows the labeling and classification of the fishes. The software solution is embedded in an online course at the Massive Open Online Course platform *edx.org* and developed additionally as a standalone website. The labeled data will be saved in the same XML format as in the *LabelImage* software. Thus the extraction module of the software can be reused for the labeled patches in the web based software. The students will be evaluated by the number of labeled fishes, with an especially developed evaluation software of the team project. For the evaluation a reference image is used in which the fishes are already identified by the experts of the GCI. If the results are satisfying it can be assumed that the following images will be labeled equally well. These data contributes to the machine learning for the automatic identification of the fishes. The online course will be repeated every eight weeks to collect training images for the *FishNet* project. During the first two weeks after the activation of the course at the platform edx.org over 300 participants took part in the course. Thereby over 13500 fishes were found in 600 images. In comparison to that, the experts of the *FishNet* team labeled 5358 fishes in four weeks. The experts first selected eleven fish species that the participants could then associate with the fishes in the pictures. In average the participants labeled 80% of the pictured fishes and associated 25% to a fish species.

Conclusion and Outlook

In summary it can be said that fishes can be labeled and classified in images with the *LabelImage* software solution by the scientists and with the web based software solution by other participants. With the evaluation software participants from the online course and the standalone website can be evaluated and the labeled fishes can be processed for the machine learning. Using these images the software can be trained and the classification of the fishes will be optimized. The software solution for identifying the fishes should facilitate the work of the scientists from the GCI. They do not have to classify the fishes manually anymore. With the underwater images from the *XL Catlin* project and the software solution the changes of the fish population in the coral reefs all over the world can be captured faster. The machine learning can be also used for detecting other objects in images, if there are enough training images available. Therefore any images can be loaded to the *LabelImage* software and then the desired objects can be labeled and classified.

Automatic detection of context information in images with machine learning

Patrick Mutter, Matthias O. Franz, Michael Grunwald

Machine learning provides several methods for image classification. We compare two methods of them to classify and detect content in images automatically. Two image datasets HIM-10.1 and HIR-10.1 are created. HIM-10.1 uses 60.000 images from existing public datasets, that matches the defined classes, while HIR-10.1 is built of 100.000 images under creative common license. As first approach support vector machines using histograms of oriented gradients as feature descriptors, are used to classify the images. Therefore, its need to find useful parameters to calculate hog-descriptors that describes all classes well. With convolutional neural networks a modern approach from deep learning is used to classify the image data. Using Nesterov-Momentum other hyper parameter and convenient model are searched to reach a good detection ratio. Finally we show that using CNNs with the datasets need less preprocessing and reach better results than SVMs with HOG-descriptors.

Introduction

Digital cameras are used in a large variety of scientific and industrial applications. For most applications the acquired data should represent the real light intensity per pixel as accurately as possible. However, digital cameras are subject to different sources of noise which distort the resulting image. Noise includes photon noise, fixed pattern noise and read noise. These noise sources are dependent on various camera parameters, for example exposure time or sensor temperature. The aim of the radiometric calibration is to improve the quality of the resulting images by reducing the influence of the various types of noise on the measured data.

A commonly used calibration technique to remove noise is the flat field correction, also referred to as flat fielding. By assuming a linear pixel characteristic flat field correction corrects the pixel-to-pixel sensitivity. Flat field correction does not reflect the non-linearity of the dark current behavior or the full-well capability. Additionally, the ability to include random noise such as photon shot noise in the calibration process is very limited when using this classical method.

To take account of the non-linear pixel behavior, regression methods which allow for more flexible modeling should be used. Regression models estimate the correct intensities of the image pixels based on observed intensities and known camera parameters. One method that can be used is Gaussian processes regression – a supervised and non-parametric machine learning technique – which allows for modeling the characteristic of individual pixels or groups of pixels dependent on various camera parameters. Gaussian processes are used because they adapt well to non-linear data which is under Gaussian noise. Additionally, only a few hyperparameters need to be optimized which can be done with gradient based optimization.

More precisely, Gaussian processes are used to model the mapping from exposure time and sensor temperature to real light intensity based on training data. This data should cover all achievable values of these three image parameters. In calibration, the real light intensity can be predicted for each pixel based on the trained regression model. Due to the computational complexity, standard Gaussian process regression is not suitable for applications which require a fast calibration.

We present a new approach for the calibration of digital cameras using sparse Gaussian processes. The sparse regression approach allows for faster training and calibration. Sparse Gaussian process regression uses a set of pseudo-inputs as additional parameters. These pseudo-inputs are derived from the original training data. The aim is an approximation for the complete training data set.

Using one regression model for each pixel raises high computational costs. Therefore the data needs to be split into a meaningful subset. The resulting quality as well as the required computation time for training are dependent on this step. We evaluated three different methods (1) one regression model per pixel, (2) one global regression model over all available images and (3) one regression model per cluster.

For our experiments we use a data set of images (256 images, each having 10 megapixels) sampled in equal intervals of real light intensity, exposure time and sensor temperature. The results show that the per pixel and global data selection are not suitable for image calibration. Due to the large amount of data the per pixel method is not realizable without special hardware – per image, 10 million regression models need to be trained. The global data selection makes the assumption that pixels at the same geometric location have equal characteristics. This is only true for some noise sources such as vignetting. Other noise sources (e.g. dark current and dirt or dust on the optical device) are not included in this model. For the final approach, pixels with equal characteristic are grouped into clusters. The characteristic of a pixel is defined by pixel value, exposure time and sensor temperature. Since in each cluster the behavior of all pixels is similar it is sufficient to take only one representative pixel per cluster over all images for training. For each cluster an individual Gaussian process regression and model selection is done. Calibration is performed by interpolating the gray-scale value of each pixel with the regression model of the respective cluster.

The experimental results show that calibration with sparse Gaussian processes is more accurate compared to classical flat field correction. We achieve a consistently higher reconstruction quality for the same overall number of calibration frames. In addition the calibration is faster than the standard Gaussian process approach. Important parameters for the proposed algorithm are the number of clusters and number of pseudo-inputs. The number of clusters can be set according to the camera system used. It influences data selection time and training time as well as the quality of the results. A lower number of pseudo-inputs results in faster training and calibration but a lower reconstruction quality.

Bibliography

[1] Masaaki Tsujitani and Yusuke Tanaka. Cross-validation, bootstrap, and support vector machines. Advances in Artificial Neural Systems, 2011.

[2] Tran Son Hai, Nguyen Thanh Thuy, et al. Image classification using support vector machine and artificial neural network. International Journal of Information Technology and Computer Science (IJITCS), 4(5):32, 2012.

[3] Navneet Dalal and Bill Triggs. Histograms of oriented gradients for human detection. In Computer Vision and Pattern Recognition, 2005. CVPR 2005. IEEE Computer Society Conference on, volume 1, pages 886–893. IEEE, 2005.

[4] Alex Krizhevsky, Ilya Sutskever, and Geoffrey E Hinton. ImageNet Classification with Deep Convolutional Neural Networks, 2012.

[5] Patrick Mutter. Automatische Bestimmung von Kontextinformationen aus Bildern mit maschinellem Lernen, 2016.

[6] Alex Krizhevsky and Geoffrey Hinton. Learning multiple layers of features from tiny images, 2009.

[7] Matthias Hermann. Methoden des Deep Learning im Bereich Convolutional Neural Networks, 2015

[8] Yann LeCun. `https://www.reddit.com/r/MachineLearning/comments/25lnbt/ama_yann_lecun/chizd8g`, 23.03.2016

[9] Nitish Srivastava, et al. Dropout. A simple way to prevent neural networks from overfitting, 2014.

The mSTAR Mission: Testing Special Relativity in Space

Thilo Schuldt, Klaus Döringshoff, Norman Gürlebeck, Sven Herrmann, Achim Peters, and Claus Braxmaier

The proposed space mission mini Space-Time Asymmetry Research (mSTAR) aims at a test of special relativity by performing a clock-clock comparison experiment in a low-Earth orbit. Using clocks with instabilies at or below the $1 \cdot 10^{-15}$ level at orbit time, the Kennedy-Thorndike coefficient will be measured with an up to two orders of magnitude higher accuracy than the current limit set by ground-based experiments. In the current baseline design, mSTAR utilizes an optical absolute frequency reference based on molecular iodine and a length-reference based on a high-finesse optical cavity. Current efforts aim at a space compatible design of the two clocks and improving the long-term stability of the cavity reference. A Phase A study has shown the feasibility of accommodating the experiment on a SaudiSat 4 bus.

Introduction

Special Relativity is classically tested by performing three types of experiments, investigating the orientation-dependence of the speed of light (Michelson-Morley experiment), the boost-dependence of the speed of light (Kennedy-Thorndike experiment) and the effect of time dilation (Ives-Stilwell experiment). The proposed mini Space-Time Asymmetry Research (mSTAR) space mission will perform a KT experiment in space by comparing an absolute (iodine-based) frequency reference to a length-based frequency reference (i.e. a laser frequency stabilized to a cavity) – both with frequency instabilities at or below the $1{\cdot}10^{-15}$ level at orbit time. This allows to determine the Kennedy-Thorndike (KT) coefficient with an up to two orders of magnitude higher accuracy than current ground-based experiments.

Performing the experiment in space offers mainly two advantages. The velocity modulation is a factor of ten higher, compared to a ground based experiment and the (putative) science signal is shifted to Fourier frequencies where the stability of oscillators is better compared to sidereal frequencies. Further, space offers a vibration free environment and elimination of large DC gravity forces.

In the baseline design, mSTAR utilizes an absolute frequency reference based on a hyperfine transition in molecular iodine near 532 nm. A frequency-doubled Nd:YAG laser is foreseen as laser that is stabilized to the iodine reference. Part of the fundamental (1064 nm) stabilized laser light is split off and sideband locked to the resonance frequency of a high finesse optical cavity made of ultra-low expansion (ULE) glass using an electro-optic modulator (EOM). This way, the frequency difference between the absolute and the length reference can be extracted from the EOM sideband frequency, which is then analyzed with respect to variations at the orbit frequency for obtaining the KT coefficient.

The mSTAR iodine clock is based on a DLR-funded setup on Engineering Model (EM) level, realized at the University of Applied Sciences (HTWG) Konstanz in cooperation with the Humboldt-University Berlin. A frequency stability below $5{\cdot}10^{-15}$ at integration times between 10 s and 5000 s was demonstrated. The length reference is based on the space-qualified cavity setup under development at JPL within the GRACE follow-on mission. A design with adapted thermal shielding required for improved long-term stability and fiber coupling to the cavity is currently realized at Stanford University.

The mSTAR mission is investigated in an international collaboration including the King Abdulaziz City for Science and Technology (KACST, Riyadh, Saudi-Arabia), Stanford University (USA), NASA Ames (USA) and a German Team consisting of the German Aerospace Center (DLR Institute of Space Systems, Bremen), the Center of Applied Space Technology and Microgravity (ZARM, University Bremen) and the Humboldt-University Berlin. In an ongoing Phase A study, the feasibility of the payload accommodation within the SaudiSat 4 satellite bus is evaluated.

Payload Overview

An overview over the mSTAR payload is given in the functional diagram shown in figure **??**. One solid-state Nd:YAG laser with a wavelength of 1064 nm is used as light source for both frequency references. The iodine reference consists of a beam preparation unit, a spectroscopy unit and corresponding locking electronics. The laser output is sent to the beam preparation unit generating pump and probe beam for the iodine spectroscopy. A secondary laser output is delivered to a modulation bench preparing the laser light for the cavity setup. As standard Pound-Drever-Hall method for cavity frequency stabilization can not be applied due to the frequency offset between the iodine and cavity resonance frequencies, an electro-optic modulator is used employing sideband locking. The feedback signal to the EOM sideband frequency is analyzed with respect to a possible KT signal at orbit frequency.

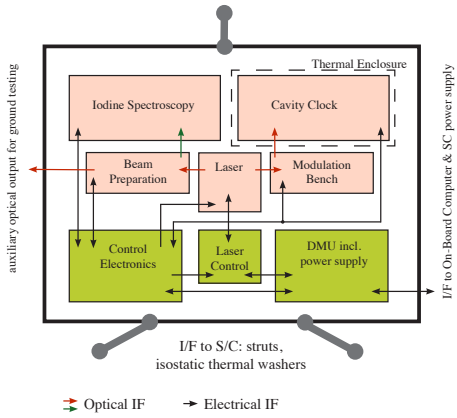

Figure 11: Functional diagram of the mSTAR payload.

The development of a space compatible iodine frequency reference setup is carried out in a cooperation of ZARM Bremen, DLR Bremen, University of Applied Sciences Konstanz, Airbus D&S Friedrichshafen and the Humboldt-University Berlin. A compact and ruggedized setup of the spectroscopy unit on engineering model (EM) level was realized, see figure **??**. The optical components are joined to a fused silica baseplate using adhesive bonding technology in combination with a space-qualified two-component epoxy. This technique allows for higher long-term stability of the iodine frequency reference due to reduced pointing instability, which is a limiting effect in standard setups. The setup takes into account space mission related criteria such as compactness, MAIVT (manufacturing, assembly, integration, verification and test) and robustness with respect to shock, vibration and thermal stress. It utilizes a specifically designed multi-pass iodine cell in nine-pass configuration. The cell has dimensions of $100\times100\times30\,\mathrm{mm}^3$ resulting in an interrogation length of approximately 90 cm and utilizes a specifically designed robust cold finger design. With this setup, a frequency stability of $7{\cdot}10^{-15}$ at an integration time of 1 s and below $5{\cdot}10^{-15}$ at integration times between 10 s and 5000 s, was demonstrated in a beat measurement with a second laboratory setup of an iodine frequency reference. This frequency stability is similar to the one of the best current state-of-the-art laboratory setup of an iodine-based frequency reference [**?**].

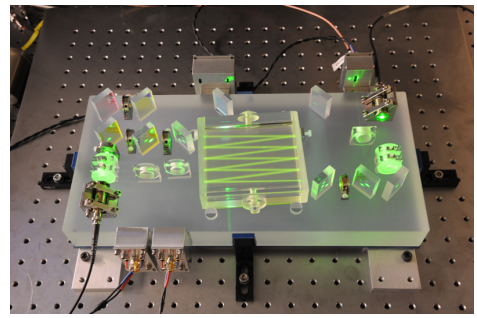

Figure 12: Photograph of the iodine spectroscopy setup.

The mSTAR baseline design for the cavity-based frequency reference foresees a mid-plane mounted cavity with a finesse > 160.000 made of ultra-low expansion (ULE) glass with a coefficient of thermal expansion (CTE) of $\sim 10^{-9}$/K within an operating temperature range of 10 – 30°C and a CTE zero crossing near 15°C. By operating the cavity close to the CTE null, the effective CTE can be further decreased. Mirror substrates are made of fused silica in order to reduce thermal noise and ULE compensation rings are foreseen in order to maintain the CTE zero crossing temperature. The thermal enclosure consists of 4 gold coated aluminum cans with titanium alloy supports. Thermal simulations yield to an attenuation factor $> 10^{10}$, so that a 1 K temperature swing at the outer shield will have negligible stress effect on the cavity.

Bibliography

[1] T. Schuldt et al.: An Ultra-Stable Optical Frequency Reference for Space, Proceedings of the 10th International Conference on Space Optics (2014)

A parallel hash map for LOD-aware depth-map fusion

Markus Friedrich, Bernd Hamann[1], Oliver Deussen[2], Georg Umlauf

We introduce a real-time and memory-efficient solution to the problem of depth-map fusion and level-of-detail aware (LOD-aware) spatial data storage. Image-space 3-d reconstruction methods result in a set of view-dependent depth-maps. In most cases, an additional depth-map fusion mechanism in combination with a spatial data storage scheme is employed to assemble and store complete 3-d models. Our approach guarantees memory efficiency by using a sophisticated hash mapping approach that can distinguish different data LODs depending on the data resolution of the input depth-maps. It is inherently better suited for modern graphics processing units (GPUs) than tree-based data structures and allows for efficient iterative data updates. The described depth-map fusion method is optimized for massive parallel processing which enables real-time performance. An evaluation of our depth-map fusion and spatial data storage solution demonstrates its applicability in the field of real-time 3-d reconstruction.

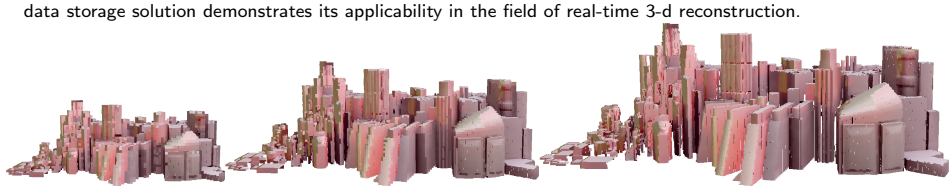

Figure 13: Renderings of a city voxel model stored at different level of details. The discussed data structure scheme exploits depth-map resolution and object-sensor distance for level-of-detail-aware, memory-efficient spatial data storage. This can be achieved without loss of geometric detail.

Introduction

In the context of image-space 3-d reconstruction, most systems implement a process pipeline consisting of three steps. In the first step a depth-map is computed and de-noised based on calibrated camera images. In the second step, the fusion step, depth-map samples are integrated into a consistent and complete 3-d model. Some approaches apply additional refinement algorithms to the model that improve surface smoothness or model water-tightness [1, 2]. The third step stores the generated surface geometry in a specialized data structure optimized for spatial information.

For real-time reconstruction systems, computational efficiency is an additional requirement for the development of the fusion algorithm and its implementation. Its solution is always a trade-off between speed and result quality. The amount of computed surface data for dense reconstruction methods exceeds that of feature-based reconstruction methods by far. This implies strict requirements on the used spatial data structure. It should provide both, memory efficient data storage and run-time efficient data insertion and retrieval. Memory efficiency can be achieved by considering sparse data structures which, unlike grid-based solutions, do not occupy memory to represent empty space. LOD strategies, which store fusion data dependent on the depth-map resolution, can further streamline overall memory consumption. To achieve run-time efficiency, the massive parallel hardware architectures of modern GPUs can be used. They allow for real-time 3-d reconstruction without specialized and thus expensive hardware. Their potential can be exploited if all used algorithms and data structures minimize global thread synchronization and per-thread operation complexity. A survey of parallel programming models and tools was published in [3].

The fusion data structure should offer parallel voxel insertion and retrieval operations as well as a sparse and LOD aware storage scheme for memory efficiency. Due to the iterative nature of the fusion process, the used data structure should guarantee constant per-iteration insertion performance. The fusion process itself should be efficient enough for real-time depth-map fusion. It should provide ef-

[1]University of California, Davis, USA
[2]University of Constance, Germany

ficient strategies for depth-map overlap detection and removal.

Current Status

Our reconstruction process consists of three steps, see Figure **??**: In the first step a depth-map based on a stream of camera images is computed. Selected images are used to estimate corresponding camera poses. The plane-sweep method computes a depth-map which is de-noised for artifact removal. In the second step depth-maps are fused into a 3-d voxel model. In the third step generated voxels are inserted into a hash map-based data structure.

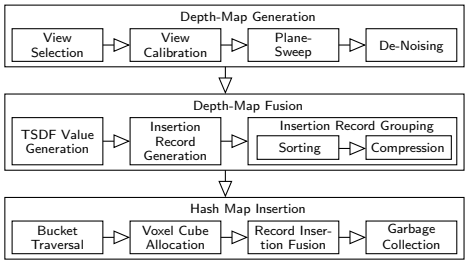

Figure 14: The three steps of the reconstruction pipeline.

This project introduces a parallel hash map data structure which is optimized for massively parallel hardware and sparse spatial voxel data. It is LOD-aware and addresses the problems of standard hierarchical approaches in terms of implementation complexity, meta-data overhead and flexibility. Unlike many other hash mapping techniques, it is well suited for iterative insertion scenarios.

The described depth-map fusion scheme parallelizes depth-map processing and addresses the problem of depth.map overlap using a simple and efficient merging strategy. To generate depth-maps we use calibrated video images as input. A single depth-map is computed based on three input images using the so-called plane-sweep method. It uses a corresponding point search with a color-based correlation measure in combination with a plane-based approach to exploit the epipolar geometry of the camera views for higher efficiency. The fusion scheme is applicable to real-time reconstruction and integrates with the underlying hash map structure.

In this project we made the following specific contributions:

- A parallel hash map data structure that supports different data LODs and is optimized for incremental insertion.
- A parallel fusion scheme that is optimized to exploit the performance of our hash map data structure.

Both contributions enable real-time depth-map fusion by exploiting the parallel processing capabilities of modern GPUs. For the fusion process we define real-time behavior

Results and Future Work

For the evaluation we used an Intel Core i7-870 quad-core processor with 8GB of available DDR3 system memory and a NVidia GeForce GTX 470 with 1280MB GDDR5 RAM. Figure **??** shows renderings of voxel models of the city model from [4] for different level of details leading to 240; 1920; 15360 allocated voxel cubes.

The evaluation results show the real-time suitability of the depth-map fusion and voxel retrieval process. The fusion process scales well with the number of allocated voxel cubes and hash map records. Thus, the hash map record insertion is the most time-consuming part of the fusion pipeline.

For future research we plan several possible extensions and improvements. The degree of parallelism decreases for an adverse ratio between number of insertion records and number of compressed insertion records. Splitting compressed insertion records that correspond to a large number of insertion records increases the degree of parallelism. In the current design, existing voxel data is completely erased when the LOD of its record is increased. A more elaborate approach could convert existing data to the new LOD preserving information.

Bibliography

[1] Zach C.: Fast and high quality fusion of depth maps. *ICCV* (2008).

[2] Zach C., Pock T., Bischof H.: A globally optimal algorithm for robust TV-L1 range image integration. *ICCV* (2007), 1–8.

[3] Diaz J., Munoz-Caro C., Nino A.: A survey of parallel programming models and tools in the multi and many-core era. *IEEE Trans. Parallel and Distributed Systems 23*, 8 (2012), 1369–1386.

[4] Crane K.: Keenan's 3d model repository. `http://www.cs.columbia.edu/~keenan/Projects/ModelRepository`, 2014. [Online; accessed 10/31/2014].

3D Primitive Classification Using Stacked Autoencoders

Merlin Blume, Pascal Laube, Matthias O. Franz, Oliver Deussen & Georg Umlauf

This work is dedicated to the recent developments in the field of deep learning. Focusing specifically on the discipline of unsupervised representation learning, five different types of regularized deep autoencoders have been evaluated on their 3D object classification capabilities. While each autoencoder scored with a positive classification rate of above 99%, convolutional neural networks initialized by autoencoders achieved the best score with 99,8%. The used training data contained six different types of primitives (planes, cylinders, cones, spheres, ellipsoids and tori) with varying parametrization and arbitrary transformations per object. Because there is a lack in publicly available labeled point cloud data, each primitive needed to be sampled synthetically. Finally three visualization techniques were implemented to qualitatively inspect each autencoder's hidden layer weights. Their analysis revealed interesting structures similar to those in the domain of 2D computer vision.

The manufacturing process of complex entities (like cars or airplanes) involves many different stages within the construction cycle. One of the most important parts is the digital engineering phase supported by key technologies like CAD & CAE. Especially in case of organic free-form surfaces digital design and reverse engineering operate hand in hand. Although the discipline of reverse engineering is primarily known in the context of product piracy there are many serious applications making it indispensable in production, whether it be the reconstruction of lost digital blueprints, the use of rapid prototyping with clay models or quality assurance matching manufactured parts against their digital copy.

In addition 3D scanning procedures have become more precise, faster and even cheaper. During the scanning, which can be based on contact sensors or optical systems, numerical data describing discrete 3D positions get sampled. The resulting Cartesian pointclouds serve as primary product for the reproduction of digital assets. This is where it gets tricky. Lots of algorithms have been developed for the extraction of approximating meshes. The conversion to mathematical surface descriptions however still depends very much on manual fine-tuning.

We attempt the experiment to go one step further in the direction of process automation. Therefore we will make use of modern concepts related to the field of machine learning. Within the last years the buzzword "big data" gained lots of attention. It is describing nothing less than a change in paradigm in our information-driven society. The trend departs from the pure analytical approach to the examination of huge databases. The amount and quality of data, but also nowadays computational power make a variety of new applications possible. Using intelligent systems, the manufacturing industry can benefit from the latest developments as well. Such algorithms learn autonomously and can easily adapt to unseen new data. Focusing on reverse engineering we will explore a method to detect and classify primitive shapes for the later extraction of mathematical bodies.

The discipline of deep learning lately gained a lot of interest in diverse fields of application. While its popularity and the fast evolvement of new techniques is quite desirable, it also raises the entry hurdle for inexperienced scientists at the same time. As a consequence one of our primary goals was to establish a good understanding for deep learning and some of the fundamentals one requires to fully grasp the overall challenges that go along with machine learning. Focusing on the automatic, unsupervised extraction of concise features for the classification of 3D primitives we turned our attention towards the field of representational learning, exclusively working on various implementations of autoencoders. Therefore we explored up to five types of autoencoders (AEs) and analysed their different approaches to model regularization.

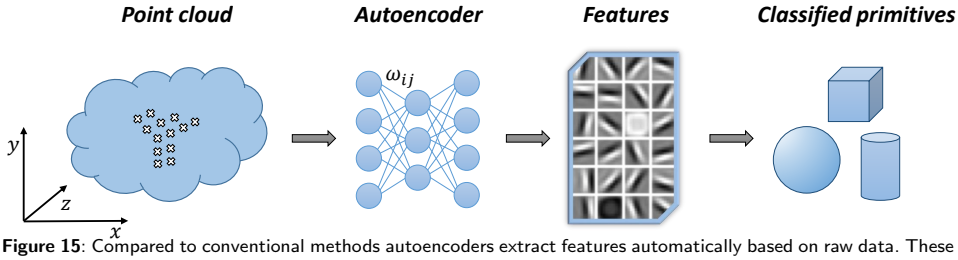

Figure 15: Compared to conventional methods autoencoders extract features automatically based on raw data. These features in turn build the foundation for final classification.

The first step to our experiments was the acquisition of training data. We generated a set of 50.000 randomly affine transformed pointclouds. As always with machine learning, data preprocessing was of mayor importance, since all point clouds varied in their number of samples and didn't possess any intrinsic consistent structure. To overcome this problem we decided to voxelize each point cloud generating regular rectangular grids. Normalizing the count of embodied points within each cell to a value in the range of $[0, 1]$ our object representation provided a 3D equivalent to 2D grayscale images. While the voxelization step led to transition and uniform scaling invariance, it did not eliminate the effect of arbitrary rotations. Experimenting with PCA and the objects' moment of inertia, we were able to sufficiently well align objects of the same type. However, to accommodate the idea of raw data processing without the slightest induction of expert knowledge, we decided to abstain from this reorientation.

The comparison with established machine learning procedures like Naive Bayes, Linear Discriminant Analysis and SVMs allowed us to better judge our experiments' outcomes. SVMs achieved high classification rates, even though grid search took them a long time to find a good initialization. Limited by the number and complexity of experimental setups we still succeeded in discovering topological structures and working parametrization for all deep models. The classification with stacked AEs always surpassed our baseline scores.

In a final step we tried to judge the performance of our AEs intuitively. For this we analysed for each model a limited set of hidden layer weights visually. Hoping to identify relevant features and to raise confidence in the methods applied, we found significant structures within the weights' graphical representations. Unfortunately they didn't allow us to fully understand what happens inside the AEs networks. Even though the features must be of importance to the machine learner, they seem to elude the visual perception of humans. Nevertheless we could spot some interesting patterns like the very frequent appearance of kidney shaped features. Considering the nature of our data and the object types they predominantly occurred with, we assume that such "kidney filters" might represent a match to 2D edge detectors. However it will take more research to check, if our interpretation is reasonable.

Vector Machines for Knot Placement in B-Spline Curve and Surface Approximation

Pascal Laube, Georg Umlauf, Matthias Franz

Knot placement for curve and surface approximation is an open problem. Selecting knot values to receive good approximation results is a challenging task. Proposed approaches range from parametric averaging to genetic algorithms. We propose the use of Support Vector Machines (SVMs) for finding suitable knot vectors in B-spline curve approximation. The SVMs are trained to be able to distinguish between locations along the curve that are well or not well suited as knots in the parametric domain. This score is based on different geometric features of a parameters corresponding point in the point cloud. A score weighted averaging technique is used to produce the final knot vector. We further propose a method to use the score weighted averaging technique for T-spline surface approximation.

Finding a good knot vector for curve and surface approximation is a common problem in many applications like e.g. Reverse Engineering (RE). In RE one starts with a sampled physical object represented by a point cloud. For this point cloud a corresponding CAD representation must be recover. After steps such as pre-processing and segmentation, a B-spline approximation of the point cloud or parts of it is computed. For this approximation the data points, parameter values for the data points, the B-spline degree, and an appropriate knot vector are required. Then the goal is to generate knot vectors that lead to approximations with as little deviation from the data set, for as few knots as possible. Usually a certain threshold has to be satisfied to assure a sufficient approximation quality. Since the number of control points is determined by the number of knots, the number of knots is especially important if the resulting curves and surfaces will be further processed by a human operator.

Because there are many unknowns in the approximation process, we propose knot vector computation using machine learning methods. We train Support Vector Machines (SVMs) to distinguish between locations along a curve that are well or not well suited as knots in the parametric domain. For training and classification we use a feature vector that concentrates information about a point clouds geometric structure. Consider a set of ordered points in two dimensional space. We define a good knot vector as the one that generates little deviation to the data set while having a small number of knots. Finding the ideal knot vector is impossible. A computationally very expensive way is to exhaustively search for appropriate knot value combinations in the set of parameters. Due to computational cost this is not feasible for practical application. Since training data has to be generated only once the cost of exhaustive search in our case is negligible. After training the SVMs are able to assign a score to each point of a point cloud based on its local point neighborhood.

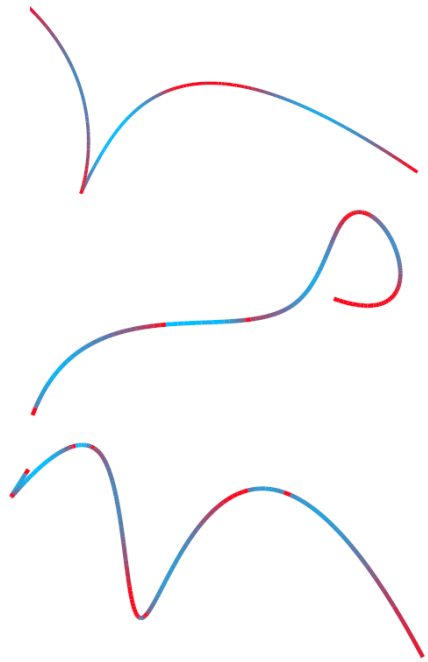

Figure 16: Three exemplar curves colored by score from high score (red) to low score (blue).

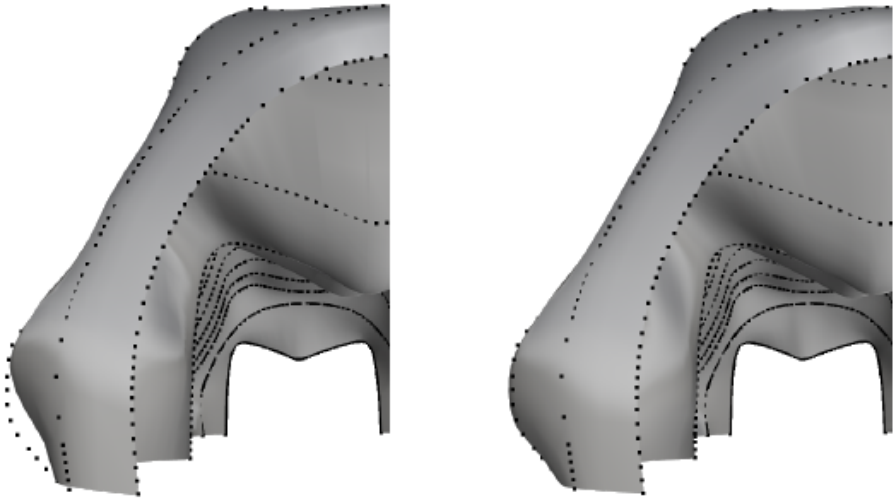

Figure 17: T-spline surface approximation by NKTP on the left and by SWKP on the right together with the original point data.

An score-weighted averaging yields then the final knot vector. This concept for B-Spline curve approximation is then applied for T-spline surface approximation. B-spline surface interpolation by surface skinning or lofting is the process of interpolation by contour curves (CCs). For an ordered set of points in which each point belongs to a serial contour along the surface one has to first interpolate points along CCs. The compatibility of the CCs needs to be ensured by degree elevation to a common degree. By interpolating the CCs one receives the lofted surface. Approximation of CCs results in an approximate lofted surface. Unordered sets of points can be converted to ordered sets for surface lofting by point cloud slicing. We propose an approach for B-spline curve and T-spline surface approximation. We train SVMs to decide on the suitability of pre-computed parameter values of a point cloud as values for a knot vector. Based on this suitability measure, or score, we perform a weighted averaging of parameter values to create the knot vector. This concept is further adapted for T-spline surface approximation by lofting. The proposed method produces approximations of good quality. This is especially the case for approximation with a small number of knots. We could show that SVMs are able to learn characteristics of positions along a curve where knot placement has positive impact on approximation quality. The approximation by lofted T-spline surfaces is able to preserve initial knot vectors of CCs and needs a fraction of the knots a comparable B-spline surface would need to satisfy a certain threshold. For future works we plan to investigate the applicability of machine learning to other steps of the RE process like point cloud segmentation. We further would like to apply deep learning techniques that render manual feature selection obsolete like e.g. neural networks with an autoencoder layer.

A Virtual-Reality 3d-Laser-Scan Simulation

Malvin Danhof, Tarek Schneider, Pascal Laube, Georg Umlauf

We present a 3d-laser-scan simulation in virtual reality for creating synthetic scans of CAD models. Consisting of the virtual reality head-mounted display Oculus Rift and the motion controller Razer Hydra our system can be used like common hand-held 3d laser scanners. It supports scanning of triangular meshes as well as b-spline tensor product surfaces based on high performance ray-casting algorithms. While point clouds of known scanning simulations are missing the man-made structure, our approach overcomes this problem by imitating real scanning scenarios. Calculation speed, interactivity and the resulting realistic point clouds are the benefits of this system.

In science and industry 3d laser scanners are widely used to acquire 3d point data of real world objects. The result of a scanning process is a 3d point cloud. Often a CAD representation of these point clouds needs to be recovered for the subsequent processing. This task is performed by the reverse engineering process. Thus, the quality of the CAD representation depends on the chosen reverse engineering process.

Figure 18: FARO Edge ScanArm (www.faro.com, 09/25/2015)

Evaluating reverse engineering algorithms is only possible if a large set of point clouds is available. To acquire these points clouds CAD models are scanned virtually. There are two reasons for this approach. First, we often lack enough suitable physical objects to scan and, second, point clouds of hand-scanned physical objects often lack corresponding CAD information. However, point clouds of hand-scanned physical objects and synthetically generated point clouds differ heavily in their structure in terms of scan-strategy and scan-path. Since each human operator has a different scan-strategy and scan-path, the resulting point clouds differ much in structure, even if the same object was scanned. On the one hand this structure is not completely random, on the other hand there is no good model for the human scanning procedure. For a fair evaluation of reverse engineering algorithms with realistic data this man-made structure must be incorporated into the data. To generate scans of CAD models that capture this man-made structure we propose a virtual reality (VR) scanner setup. We present a method to generate 3d point clouds from CAD models consisting of triangle meshes and b-spline tensor product surfaces with a simulated hand-held laser scanner in a VR environment (Fig. **??**).

Figure 19: VR setup.

Our goal is to create a realistic simulation of the scanning process with a hand-held laser scanner like the FARO Edge ScanArm (Fig. **??**). Using this approach we can compute 3d point clouds of CAD models using a virtual laser scanner with a man-made scan structure.

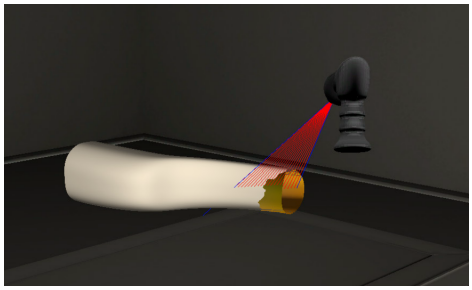

Figure 20: The virtual scene.

For the simulation of a hand-held 3d laser scanner we propose a VR environment. The structure of the synthetic point clouds generated in this VR is similar to man-made scans of physical objects due to the manual scanning process. The virtual scene consists of a workshop with a table, that carries the CAD model, and a virtual model of the scanner, see Figure **??**. The user can move freely in the scene, change the perspective and field of view in terms of the CAD model and operate the laser scanner. For the VR setup two essential peripherals are used: the VR headset Oculus Rift for visual immersion and the motion controller Razer Hydra for scanner control and scene navigation. The Oculus Rift provides a 3d view of the VR scene and allows to freely explore the 3d scene. Integrated sensors provide data about the user's head position and orientation. Due to its large field of view the degree of immersion in the scene is very high. The Razer Hydra consists of two wired controllers and a base station, which creates a magnetic field to determine the controllers' spatial positions. It can capture hand movements and orientations accurately and provides joysticks and buttons for control tasks. Both devices are integrated using the manufacturer' APIs: Oculus Rift SDK and Sixense Core API.

This solution makes scanning of CAD models inside a VR environment possible. Interaction with our system matches the process of operating a real hand-held laser scanner. The resulting point clouds cannot be differentiated from non-synthetic scans. Interactivity and execution speed of our application meet the expectations. The scan process is realistic and easy to perform. Nevertheless there are a few drawbacks. The Razer Hydra is not connected to a leading arm like some real laser scanners which leads to difficulties moving the scanner calm and precise. This could be compensated by an adjustable factor which decreases the sensitivity of the Hydra. Since the Oculus Rift is still in development there are a few points which will certainly improve with later versions. Especially the resolution causes the problem of a visible pixel grid and a blurry perception of concrete shapes on looking around in a scene. This problem will hopefully get fixed with newer versions which should have a higher pixel density.

Merging Multiple 3D Face Reconstructions

Leonard Thießen, Pascal Laube, Georg Umlauf, Matthias Franz

We present a method to merge multiple 3D face reconstructions into one common reconstruction of higher quality. The individual three-dimensional face reconstructions are computed by a multi-camera stereo-matching system from different perspectives. Using 4-Points Congruent Sets and Iterative Closest Point the individual reconstructions are registered. Then, the registered reconstructions are merged based on point distance and reconstruction tenacity. To optimize the parameters in the merging step a kernel-based point cloud filter is used. Finally, this filter is applied to smooth the merged reconstruction. With this approach we are able to fill holes in the individual reconstruction and improve the overall visual quality.

Introduction

Face recognition is an important problem in biometric applications that is usually based on two-dimensional images. However, it has been shown that the recognition rate can be improved, if the recognition is based on 3D face reconstructions. This requires an accurate and fast reconstruction method, e.g. based on real-time multi-camera stereo-matching as presented in [**?**]. The algorithm is based on four synchronized cameras which captures images of a face from different perspectives . With this system it is possible to generate high-resolution depth images in real-time. This reconstruction also contains detailed information about the reconstruction tenacity. A bad matching pixel correspondence in the computation of the depth map will result in a low tenacity value for the reconstructed 3D point. As a result, the algorithm yields one 3D reconstruction of the captured face. The main focus of this approach was on recognition rate and reconstruction speed, reconstruction quality was not the main concern. Thus, the reconstructions may be noisy or have holes.

We propose a process to merge multiple reconstructions to improve the overall visual reconstruction quality. Due to the lack of a ground truth geometry the noise level is used as an additional quality measure during the merging process.

Merging 3D Face Reconstructions

The reconstruction system used captures a face from four different angles and uses multi-camera stereo-matching to compute a 3D reconstruction. The reconstructed geometry is represented as point cloud equipped with a measure to the quantify the local tenacity of the reconstruction. For details refer to [**?**]. Due to the speed of the reconstruction process several 3D reconstructions can be computed per second. These 3D reconstructions are usually from different perspectives since the person moves.

To merge these different 3D reconstructions we propose an approach consisting of four steps. First a coarse registration of the point clouds is done using 4-Points Congruent Set (4PCS) [**?**]. It's a global registration algorithm assuming no prior knowledge of the point clouds, so they can be in a arbitrary initial pose. This is followed by a fine registration using Iterative Closest Point (ICP). This algorithm tries to minimize the squared distances between neighbor points in both point clouds. An example of the entire registration process using 4PCS and ICP is shown in figure **??**.

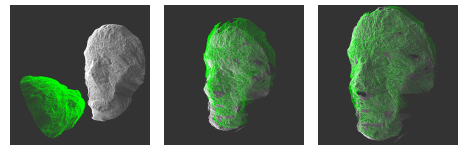

(a) (b) (c)

Figure 21: Registration of two example point clouds **??**, after applying 4PCS **??**, and after applying ICP **??**.

The third step is to merge the registered point clouds to one 3D reconstruction using tenacity weighted interpolation. Each 3D reconstruction has regions where the point positions are more or less reliable. This is due to lighting effects, relative camera positions and orientations, etc. This reliability of a reconstructed point $\mathbf{p}$ is measured by the tenacity $t(\mathbf{p}) \in [0, 1]$, which is given as some weighted normalized cross-correlation of corresponding pixel neighborhoods in the four camera images, see [**?**]. Smaller values for t indicate higher point tenacity. Having several 3D

reconstructions of the same face, a rather frontal reconstruction is usually reliable for forehead, nose, and mouth regions and unreliable for the cheeks. Thus, we chose a rather frontal reconstruction as reference reconstruction $\mathcal{P}_0$ that is enhanced and enriched be the additional reconstructions $\mathcal{P}_1, \ldots, \mathcal{P}_k$. The merged reconstruction $\mathcal{R} = \{\mathbf{r}_1, \ldots, \mathbf{r}_M\}$ is generated by adding points from one $\mathcal{P}_i, i = 0, \ldots, k$, or from a tenacity weighted interpolation of points from several $\mathcal{P}_i$ - depending on tenacity and point distances, there are five reconstruction parameters. In a last step the merged 3D reconstruction is filtered to erase noise. Due to the lack of a ground truth the result of the filter process can be used for quality measurement. If $\mathcal{R}_f = \{\mathbf{r}_1^f, \ldots, \mathbf{r}_M^f\}$ denotes the filtered reconstruction, the parameters are chosen such that $\mathcal{R}$ and $\mathcal{R}_f$ are close with respect to the error $e = \sum ||\mathbf{r}_i - \mathbf{r}_i^f||^2$, i.e. the filtering has minimal effect on $\mathcal{R}$, which denotes a high reconstruction quality. As point cloud filter we use the kernel-based filter method of Schall et al. [**?**]. Exemplary results of the filter process are shown in figure **??**.

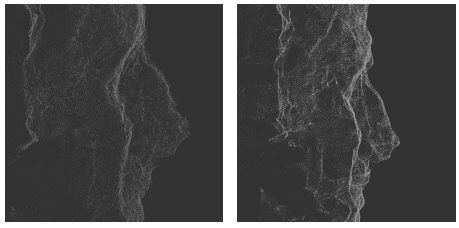

(a) (b)

Figure 22: Closeup of the nose of a joined reconstruction with optimized **??** parameters and after filtering **??**.

Next Steps

The initial reconstructions that are merged later on contain color information which at the moment is lost in the interpolation step. For future work, point color has to be included in the process. Color information could be used when deciding point neighborhood as well as for lifelike visualization.

The presented method and the resulting parameters have shown to be optimal for reconstructions generated by the stereo-matching approach in [**?**]. To prove the general applicability of our algorithm data sets of other 3D face reconstruction systems need to be evaluated. The overall algorithm has not been optimized for real-time application yet.

Bibliography

[1] Klaus Denker and Georg Umlauf. An accurate real-time multi-camera matching on the gpu for 3d reconstruction. *Journal of WSCG*, 19:9–16, 2011.

[2] D. Aiger, N. J. Mitra, and D. Cohen-Or. 4-points congruent sets for robust surface registration. *ACM Transactions on Graphics*, 27(3):#85, 1–10, 2008.

[3] Oliver Schall, Alexander Belyaev, and Hans-Peter Seidel. Robust filtering of noisy scattered point data. In *Proceedings of the Second Eurographics / IEEE VGTC Conference on Point-Based Graphics*, pages 71–77, 2005.

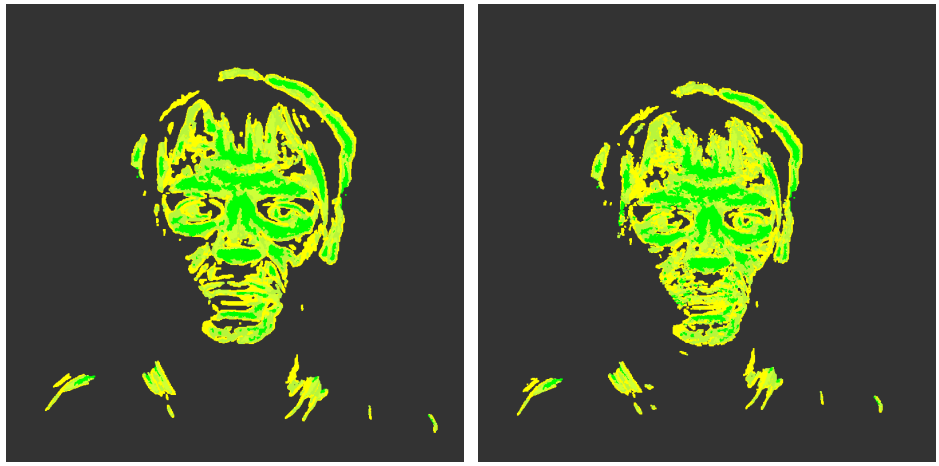

(a) (b)

Figure 23: Tenacity colored images of a reference reconstruction **??** and the the respective merged reconstruction **??**. The color gradient ranges from bright green (high tenacity) to yellow (bad tenacity).

On-line splat rendering

Marco Fehrenbach, Korkiat Khumphai, Felix Schuckert, and Georg Umlauf

Scanning real objects with the Faro Edge 3d ScanArm produces a large amount of geometrical points. Additionally during the scanning process the point cloud is able to grow dynamically or to replace a large area of points. The reconstruction of these points is very time consuming. To render a valid representation of the real object, we implemented a splat rendering process. The process uses the GPU to display the point cloud in real time. With this process the user is able to see the scanning results immediately.

Introduction

Scanning real objects is an important topic of computergraphics. An use case is to reconstruct the real object in a CAD representation. Another case is to identify the scanned object with the help of machine vision and learning. Nowadays the used hardware is very accurate and produces a large amount of useful data. For example the used Faro Edge 3d ScanArm. But the representation of the data is either very time consuming or needs additional interpretations. The solution is the implementation of a splat rendering process. The process directly uses the raw input data without any precomputations or additional requierements. Also it can handle the dynamic behaviour of the input data during the scan process. The result implementation is a part of an existing project to reconstruct CAD geometry [**?**].

Splat rendering process

The splat rendering process is based on the previous work of Botsch et. al. [**?**]. It uses the technique to expand the point size of the OpenGL pipeline. Then the normal of the point is used to discard single pixels of the point sprite. The sprite matches a rotated ellipse, which represents the surface at the point position. See figure **??**. The gray circle represents the original sprite. C is the original point and $\vec{n}$ the surface normal. Additionally, to calculate the phong lighting model, the main curvatures k1 and k2 and the directions are needed. The blue ellipse represents the result pixels to draw.

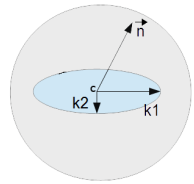

Figure 24: A single splat with the mathematical definitions

To render a large amount of points, we used an accelerating control structure. Because the input points don't move, we choose an octree implementation. The octree uses the OpenGL vertex buffer objects to send the data to the GPU. Each leaf in the tree includes a single buffer object with configurable size. If a point is added to or removed from a leaf, the octree rebuilds a single vertex buffer only. This structure is able to support frustum culling on the CPU and to reduce the workload between the main memory and the GPU memory. See figure **??** for a culling example.

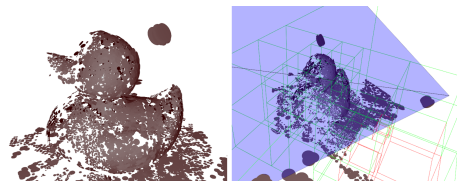

Figure 25: Left: Original camera image, right: Frustum in blue with rendered leaves in green and culled leaves in red.

Results

We used a couple of objects to validate the result of the implemented splat renderer. Figure **??**

shows an elephant toy scanned with our Faro laser scanner. The point cloud includes approximately 100.000 points.

Figure 26: Representation of an elephant toy with approximately 100.000 splats.

Also the figure shows the different scanning qualities. The abdominal area doesn't contain enough points to represent the surface completely. In contrast to the head. The difference is due to the behaviour of the user. So the user can see, which area needs more input data to be complete. The performance of the algorithm depends on the number of input data, the size of the splats and the used GPU. Because the fragment shader gets the most load in the program, using a small splat size with more points is very effective. For a few points, using a large splat size can create an invalid surface representation. See figure **??**.

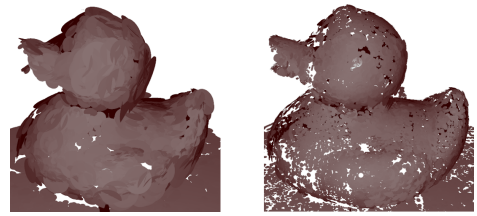

Figure 27: Representation of a duck with different number of splats and splat sizes.

Bibliography

[1] Denker, K. and Hagel, D. and Raible, J. and Umlauf, G. and Hamann, B.: On-line Reconstruction of CAD Geometry, Inter. Conf. on 3D Vision, 151-158, 2013.

[2] Mario, Botsch and Michael, Spernat and Lief, Kobbelt: Phong Splatting, Computer Graphics Group, RWTH Aachen Technical University, 2004, Presented on Eurographics Symposium on Point-Based Graphics.

Energieeffiziente Beleuchtung von Solitärobjekten

Fatih Demiralp, Gero Kern, Melanie Walde, Bernd Jödicke

Allein die Dosis macht das Gift. Was schon Paracelsus in Bezug auf Medizin feststellte, lässt sich auch ohne Weiteres auf das Thema Licht übertragen. Dies lässt sich unschwer beim Betrachten exzessiver Solariumgänger beobachten. Die richtige Dosis ist auch Untersuchungsgegenstand dieser Publikation. Wie viel Licht ist ausreichend, um ein Solitärobjekt sowohl energiesparend zu beleuchten, als auch aufmerksamkeitswirksam von seiner Umgebung abzuheben. Das Ziel dieser Projektarbeit ist die Ermittlung der optimalen Leuchtdichte, um obigen Anforderungen gerecht zu werden.

Für den Versuch wurde ein Objekt mit unterschiedlich viel Licht beschienen. Die Qualität der erzeugten Beleuchtungen wurde dann bewertet.

Als zu beleuchtendes Objekt wurde die Riesenbergkapelle in Konstanz ausgewählt. Diese eignet sich für den Versuch besonders gut, da sie sich auf der lichten Spitze eines bewaldeten Hügels befindet. Zum einen ist sie frei vom störenden Einfluss künstlicher Lichtquellen, zum anderen können die verschiedenen Beleuchtungen aus großer Distanz beobachtet und bewertet werden.

In der konkreten Umsetzung lief der Versuch wie folgt ab: Als Lichtquelle wurde eine auf einen Wertebereich zwischen $0,03 \sim cd/m^2$ und $3 \sim cd/m^2$ dimmbare LED-Leuchte verwendet. Insgesamt wurden drei Messreihen durchgeführt. Eine Messreihe umfasste fünf verschiedene Beleuchtungsintensitäten. Bewertet wurden die verschiedenen Beleuchtungsszenarien von einem Zwei-Mann-Team von einem $700 \sim m$ entfernten Standort aus. Zur Bewertung wurden Zensuren von eins bis vier vergeben. Ursächlich für eine schlechte Zensur kann sowohl eine zu geringe Leuchtdichte sein, bei der das Objekt als zu dunkel wahrgenommen wird, als auch eine zu hohe Leuchtdichte, bei der die Objektoberfläche blendend wirkt. Als Messwerte wurden sowohl die Leuchtdichte L als auch die Beleuchtungsstärke E ermittelt.

Abbildung 1 veranschaulicht die unterschiedlichen Beleuchtungsintensitäten. Sie sind der persönlichen Wahrnehmung nachempfunden dargestellt.

Das Ergebnis des Experiments (Abbildung 2) zeigt, dass sich bei $\varnothing\ 0,3 \sim cd/m^2$ ein eindeutiges Maximum einstellt. Bei dieser Leuchtdichte wird die Objektbeleuchtung als besonders angenehm empfunden. Eine Leuchtdichte von $\varnothing\ 1,82 \sim cd/m^2$ wird als zu hell und fast schon blendend wahrgenommen. Werte unterhalb einer Leuchtdichte von $0,1 \sim cd/m^2$ werden als zu dunkel bewertet. Verglichen mit dem unbeleuchteten Zustand hebt, sich ein Objekt selbst bei einer Leuchtdichte von $\varnothing\ 0,03 \sim cd/m^2$, immer noch sichtbar von seiner Umgebung ab. Die Leuchtdichte ist jedoch nicht ausreichend, um Aufmerksamkeit auf das Objekt zu ziehen. Der Bereich um $0,1 \sim cd/m^2$ stellt einen guten Kompromiss zwischen Energieeffizienz und Inszenierung dar.

Bei der Objektbeleuchtung spielt neben dem gewählten Leuchtmittel und der Intensität auch das Material eine entscheidende Rolle. Eine wichtige Kennzahl in diesem Zusammenhang ist der Reflexionsgrad ρ der Objektoberfläche. Dieser lässt sich aus der Beleuchtungsstärke E und der Leuchtdichte L bestimmen:

$$\rho = \frac{L \cdot \pi}{E}$$

Beim Untersuchungsobjekt beträgt der Reflexionsgrad 55%, dabei handelt es sich um eine Fassade aus weißem Putz. Die Größe des Objekts und das gewählte Leuchtmittel bzw. dessen Lichtausbeute η sind entscheidende Parameter bei der Berechnung der notwendigen elektrischen Leistung P. Diese lässt sich unter Zuhilfenahme der Beleuchtungsstärke E und der Fläche A wie folgt berechnen:

$$P = \frac{E \cdot A}{\eta}$$

Am Beispiel der $30\ m^2$ großen beleuchteten Front des Solitärobjekts ergibt sich bei Verwen-

dung von LED-Leuchten mit $\eta > 100 lm/W$ am Optimalpunkt (Ø 0,3 cd/m^2 bzw. 1,7 Lux) ein Leistungsbedarf von rund 0,5 W. Unter Berücksichtigung möglicher Verluste empfiehlt es sich, von einer Leistung von mindestens 1 W auszugehen. Voraussetzung hierfür ist, dass die zu beleuchtende Fläche und der Reflexionsgrad dem Untersuchungsobjekt entsprechen.

Die technische Umsetzung des Beleuchtungskonzepts kann dabei kostengünstig durch die Verwendung einer solarbetriebenen Leuchte erfolgen. Hierbei wird im Laufe des Tages ein Akku geladen, mit dem dann über die Nacht die LEDs betrieben werden. Der weitestgehend autarke Betrieb ermöglicht selbst bei sehr abgelegenen Objekten ohne Netzzugang eine optisch ansprechende Inszenierung.

Um ein Solitärobjekt optimal zu beleuchten wird eine Leuchtdichte von 0,3 cd/m^2 vorgeschlagen. Die ermittelten Werte gelten aufgrund der geringen Anzahl an Messreihen und der bewertenden Personen nur als grobe Orientierung. Weitere Versuche zur Validierung der Ergebnisse erscheinen sinnvoll.

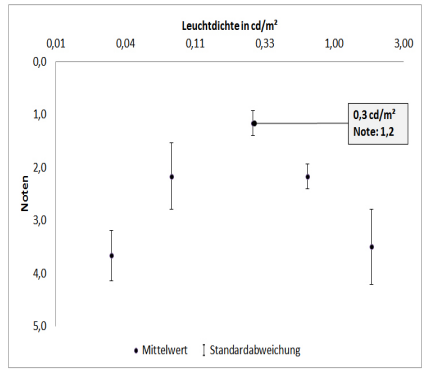

Figure 28: Untersuchungsergebnisse.

Melanopische Lichtwirkung - Aktuelle Erkenntnisse aus Forschung und Lichtplanung

Daniel Feuser, Gabriela Guillen und Thomas Scheiling

Licht und dessen biologische Wirkung ist schon seit mehreren Jahren ein wichtiges Thema. Einige namhafte Firmen sprechen sogar von der dritten Dimension des Lichts. Dennoch dürfen Begriffe wie biologische Lichtwirkung und melanopische Lichtwirkung nicht synonym verwendet werden. Dieser Artikel gibt einen Überblick über die wissenschaftlichen Grundlagen zum Thema *melanopische Lichtwirkung* und liefert erste Ansätze für eine konkrete Umsetzung in der Lichtplanung.

Licht ist für den Menschen unverzichtbar. Es verhilft uns nicht nur zum Sehen, es hat auch Auswirkungen auf unser Wohlbefinden und die Gesundheit. Unsere sogenannte "innere Uhr" wird täglich durch das Tageslicht synchronisiert und übernimmt daraufhin wichtige Steuerungsaufgaben im Körper.

Das Leben des modernen Menschen findet heute nicht mehr maßgeblich im Freien sondern überwiegend in geschlossenen Räumen mit künstlicher Beleuchtung statt. Der positive Einfluss von Tageslicht verringert sich dadurch immer mehr. Fehlt das Tageslicht, so gerät die innere Uhr aus dem Takt, was zu Schlafstörungen, chronischer Müdigkeit und im schlimmsten Fall zu Depressionen führen kann.

Tageslicht zeichnet sich insbesondere durch sein Spektrum und seine Dynamik aus. Am Morgen und am Abend, d.h. während des Sonnenaufgangs und des Sonnenuntergangs, verschiebt sich das Spektrum zu einem erhöhten Rotanteil. In der Zeit dazwischen enthält das Tageslicht einen erhöhten relativen Anteil am blauen Spektrum.

Im Jahr 2001 entdeckten Wissenschaftler spezielle Ganglienzellen auf der Netzhaut. Im Gegensatz zu den bekannten Stäbchen und Zäpfchen unterstützen diese jedoch nicht das Sehen, sondern vermitteln nicht-visuelle Reize an das Gehirn und steuern damit biologische Vorgänge im Körper [**?**]. Zu den nachgewiesenen Vorgängen zählen unter anderem [**?**]:

- Die Unterdrückung der Melatonin-Produktion
- Die Stabilisierung der inneren Uhr
- Die Steigerung des Wachheitsgrades

Diese speziellen Fotorezeptoren arbeiten mit dem Photopigment *Melanopsin* und reagieren äußerst sensibel auf Licht im blauen Spektrum. In der Fachliteratur werden lichtinduzierte biologische Vorgänge als *melanopische Lichtwirkung* bezeichnet. Diese Entdeckung verleiht der Thematik Licht eine neue Dimension. Zur eigentlichen Sehaufgabe kommt ein gesundheitlich-biologischer Aspekt hinzu, der in den letzten Jahren zunehmend diskutiert wurde. Eine *melanopisch wirksame* Beleuchtung orientiert sich am Tageslicht und bringt dadurch zusätzlich zur visuellen eine nicht-visuelle Wirkung mit sich. Eine solche Beleuchtung soll sich den jeweiligen Bedürfnissen des Menschen anpassen. Zusätzlich zur Stabilisierung der inneren Uhr wird das Leistungsvermögen und die Konzentration in den aktiven Phasen gesteigert und eine nachhaltige Regeneration in den Erholungsphasen begünstigt [**?**].

Melatonin Suppression

Das Epiphysenhormon *Melatonin* wird in den Nachtstunden im Gehirn produziert. Es fördert die Müdigkeit und kann durch seine Ausschüttung die innere Uhr beeinflussen.

Licht einer gewissen Wellenlänge und Beleuchtungsstärke ist in der Lage die Melatonin-Produktion zu unterdrücken bzw. zu vermindern. Abbildung **??** zeigt die spektrale Empfindlichkeit der Melatonin-Suppression gegenüber der bekannten spektralen Hellempfindlichkeit $V(\lambda)$. Der Punkt der größten Empfindlichkeit befindet sich bei ca. 450 nm und ist damit, verglichen mit der spektralen Hellempfindlichkeit $V(\lambda)$, ins blaue Spektrum verschoben. Eine licht-induzierte Melatonin-Unterdrückung kann folglich nur bei einer Strahlung stattfinden, deren Spektrum die

Wellenlängen zwischen 350 nm und 550 nm beinhaltet.

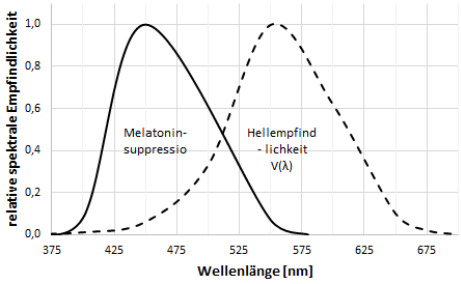

Figure 29: Wirkung monochromatischen Lichts auf die Melatonin-Unterdrückung in der Nacht verglichen zur spektralen Hellempfindlichkeit V(λ) [?].

Zusätzlich zum richtigen Spektrum erfordert die Melatonin-Suppression eine geeignete Beleuchtungsstärke. "Inzwischen ergeben neueste Untersuchungen [..], dass die 50%-Wirkungsschwellen für melanopische Lichtwirkungen wie Melatonin-Suppression, [...] zwischen 90 und 180 lx vertikaler Beleuchtungsstärke am Auge liegen" [?]. Abbildung ??a) zeigt die Ergebnisse eines Versuchs, bei dem durch eine nächtliche 6,5 Stunden dauernde Exposition mit weißem Licht[1] und 100 lx vertikaler Beleuchtungsstärke der Melatonin-Gehalt im Blut vollständig unterdrückt wurde.

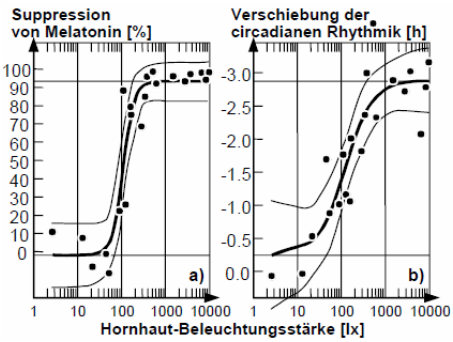

Figure 30: Lichtinduzierte Suppression von Melatonin und Verschiebung der circadianen Rhythmik auf der Zeitachse [?].

Für die Unterdrückung der Melatonin-Produktion sind jedoch noch weitere Faktoren entscheidend. So sollten zusätzlich zum Spektrum und der Beleuchtungsstärke auch die Dauer der Bestrahlung und die Richtung, aus der bestrahlt wird, erfasst und analysiert werden. Quellen belegen, dass Licht, welches von oben ins Auge fällt, die Melatonin-Produktion wirksamer unterdrückt als Licht von unten [?]. Weitere Einflüsse wie intermittierendes Licht können den folgenden Quellen entnommen werden [?] [?] [?] [?].

Stabilisierung der inneren Uhr

Die innere Uhr, oder fachlich der circadiane Rhythmus, beschreibt einen biologischen Rhythmus mit einer Periodendauer von etwa 24 Stunden. Er steuert wichtige Funktionen im Körper, wie beispielsweise die Herzfrequenz, die Körpertemperatur oder den Schlaf-Wach-Rhythmus.

Licht ist einer der wichtigsten Taktgeber für die Synchronisation der circadianen Rhythmik auf die 24 Stunden eines Tages. Die Zirbeldrüse im Gehirn beginnt am Abend damit, Melatonin auszuschütten, wobei von zwei bis drei Uhr morgens der Höhepunkt erreicht ist und der Melatonin-Gehalt im Blut dann wieder absinkt (Abbildung ??).

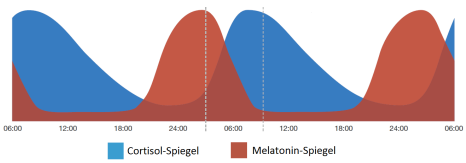

Figure 31: Beispielhafter Cortisol- und Melatonin-Verlauf [?].

Es ist nachgewiesen, dass geeignetes Licht zur richtigen Zeit den circadianen Rhythmus in der Zeit und der Amplitude verschieben kann [?]. Licht am späten Abend verzögert demnach die innere Uhr, da dem Körper signalisiert wird, es wäre noch Tag. Licht am frühen Morgen hingegen beschleunigt den Rhythmus. Analog zur Melatonin-Suppression konnte diese Lichtwirkung ebenfalls mit einer nächtlichen 6,5 stündigen vertikalen Lichtexposition mit weißem Licht[1] bei 100 lx am Auge nachgewiesen werden (Abbildung ??b) [?]. Geeignete Werte für die Praxis werden derzeit untersucht. Forscher halten es jedoch für möglich, dass bereits das Überschreiten einer Wirkungsschwelle von 30 lx am Auge über mehrere Tage hinweg für die Stabilisierung des circadianen Rhythmus ausreicht [?].

[1] "Light was generated using overhead cool white fluorescent lamps (North American Philips Lighting, Bloomfield, NJ, USA) filtered with a Lexan 9030 UV restricting lens (General Electric Plastics, Pittsfield, MA, USA) and designed to provide uniform illuminance to the whole experimental room (Philips Lighting, The Netherlands). [?]"

Steigerung des Wachheitsgrades

Im Laufe eines Tages werden im menschlichen Körper unterschiedliche Hormone ausgeschüttet; morgens bei Tageslicht *Serotonin* und bei Dunkelheit am Abend *Melatonin*.

Das Hormon Serotonin wirkt stimmungsaufhellend und motivierend. Im Gegensatz zu Melatonin, welches den Menschen müde macht, verhilft Serotonin zu mehr Leistungshochs. Außerdem ist es sehr wichtig für die Melatonin-Produktion, da dieses in zwei Schritten aus der Aminosäure Tryptophan und Serotonin synthetisiert wird. Daraus kann gefolgert werden, dass genügend Serotonin am Tag die Melatonin-Ausschüttung in der Nacht positiv beeinflusst, wodurch ein tieferer und erholsamerer Schlaf gewährleistet werden kann.

Besonders in den Wintermonaten, in den Tagesrandstunden oder in schlecht ausgeleuchteten Räumen kann die Serotonin-Produktion gestört sein. Spezielle Lichttherapien oder Lichtduschen können die gezielte Ausschüttung von Serotonin bewirken und damit den Wachheitsgrad und die Leistungsfähigkeit steigern. Diese Konzepte sind in ihrem Spektrum und der Beleuchtungsstärke meist dem Tageslicht nachempfunden. Quellen belegen jedoch, dass ab etwa 100 lx Beleuchtungsstärke am Auge die subjektive Ermüdung sinkt bzw. die subjektive Munterkeit steigt [**?**] (Abbildung **??**).

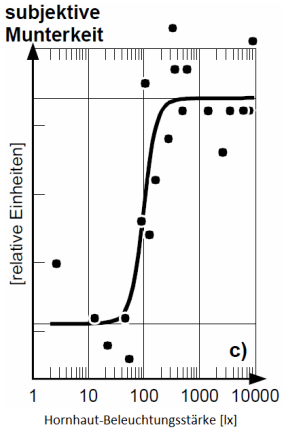

Figure 32: Subjektive Munterkeit [**?**].

Planungsempfehlungen

Auch die Lichtindustrie hat das Potenzial von melanopisch wirksamer Beleuchtung erkannt und erweitert dahingehend Ihr Produktportfolio. Die nächste Hürde besteht nun darin, diese Produkte korrekt einzusetzen, um auch die gewünschte Wirkung zu erzielen.

Die Planung einer melanopisch wirksamen Beleuchtung ist sehr anspruchsvoll und kann nur mit Hilfe eines ganzheitlichen Licht- und Raumplanungskonzepts realisiert werden. Die nichtvisuelle Lichtwirkung hängt insbesondere vom Zusammenspiel der Faktoren Lichtspektrum, Beleuchtungsstärke, Lichtverteilung und Dynamik ab. Dementsprechend gilt für eine melanopisch wirksame Beleuchtung [**?**]:

- Lichtspektrum: Kurzwelliges blaues Licht (ideal: 450nm).
- Beleuchtungsstärke: Ab etwa 100 lx am Auge (Konkrete Werte werden noch erforscht).
- Lichtverteilung: Großflächig verteiltes und von oben fallendes Licht, damit die malanopsinhaltigen Ganglienzellen im unteren und nasalen Bereich der Netzhaut erreicht werden.
- Dynamik: Zeitliche Änderungen des Spektrums, der Beleuchtungsstärke und der Lichtverteilung erhöhen die melanopische Lichtwirkung.

Es gilt: Das richtige Licht zum richtigen Zeitpunkt. Ein melanopisch wirksames Beleuchtungssystem muss sich an den circadianen Rhythmus und die individuellen Bedürfnisse des Nutzers anpassen.

Konkrete Planungsempfehlungen sind in der Norm DIN SPEC 67600 beschrieben. Dabei wird über die Gestaltung einer melanopisch wirksamen Beleuchtung für unterschiedliche Anwendungen (u.a. Pflegeheime, Ausbildungsstätte, Gesundheitseinrichtungen, Arbeitsplätze mit Schichtarbeit) informiert. Konkret empfiehlt die Norm für eine aktivierende Wirkung ein großflächig verteiltes Licht mit hohen Blauanteilen sowie einer Beleuchtungsstärke von 250 Lux bei 8.000 Kelvin Farbtemperatur [**?**]. Kritische Stimmen halten diese Werte jedoch für aus der Luft gegriffen und schwer umzusetzen.

Ein ganzheitliches Lichtkonzept für die Umsetzung in der Praxis ist beispielweise das Human Centric Lighting Konzept (HCL-Konzept) [**?**]. Dabei sorgen moderne Lichtquellen für das gezielte Lichtspektrum, Leuchten und Raumgestaltung für die Lichtverteilung und Lichtsteuerungssysteme für die Dynamik.

Das Angebot in diesem Bereich wächst. Lichtlösungen wie die Active Leuchten von TRILUX, Arktika-P Biolux von OSRAM sowie komplette Beleuchtungssysteme wie das HealWell von Philips sind nur einige Beispiele der Produkte,

die aktuell am Lichtmarkt für verschiedene Anwendungsbereiche angeboten werden. Auch namhafte Hersteller wie z.B. Waldmann, Zumtobel und Siteco arbeiten an vielversprechenden Konzepten. Bei all diesen Konzepten ist jedoch zu beachten, dass die zugrundeliegende melanopische Lichtwirkung noch nicht vollständig erforscht und die resultierenden Wirkungen noch nicht abschließend belegt sind. Bis dato sind auch weiterhin Lichtlösungen, bei denen die melanopische Lichtwirkung nicht miteinbezogen wird, Stand der Technik.

Bibliography

[1] Schierz Ch.: Unspezifische biologische Lichtwirkungen am Arbeitsplatz. (2002)

[2] Deutsches Institut für Normierung: Biologisch wirksame Beleuchtung - Planungsempfehlungen. DIN SPEC 67600, Berlin, Beuth Verlag (2013)

[3] Lasko T.A., Kripke D.F., Elliot J.A.: Melatonin suppression by illumination of upper and lower visual fields. J. Biol. Rhythms V14 N2 (1999) P122-125.

[4] Rimmer D.W., Boivin D.B., Shanahan T.L., Kronauer R.E. et al.: Dynamic resetting of the human circadian pacemaker by intermittent bright light. Am. J. Physiol. Regulatory Integrative Comp. Physiol. V279 (2000) P:R1574-R1579.

[5] Visser E.K., Beersma D.G.M., Daan S.: Melatonin suppression by light in humans is maximal when the nasal part of the retina is illuminated. J. Biol. Rhythms V14 N2 (1999) P116-121.

[6] Zeitzer J.M., Dijk D.-J., Kronauer R.E., Brown E.N., Czeisler C.A.: Sensitivity of the human circadian pacemaker to nocturnal light: melatonin phase resetting und suppression. J. Physiol. V526.3 (2000) P695-702.

[7] Cajochen C., Zeitzer J.M., Czeisler C. A., Dijk D.-J: Dose-response relationship for light intensity and ocular and electroencephalographic correlates of human alertness. Behav. Brain Res. V115 (2000) P75-83.

[8] Wang J.Y., Hanifin J.P., Rollag M.D., Brainard G.C.: Ocular regulation of the human pineal gland: The significance of total retinal exposure for melatonin suppression. Biologic Effects of Light 1998, Kluwer Boston (1999) P367-373.

[9] Gaddy J.R., Ruberg F.L., Brainard G.C., Rollag M.D.: Pupillary modulation of light-induced melatonin suppression. Biologic effects of Light 1993. W. de Gruyter, Berlin (1994) P159-168.

[10] Jewett M.E., Rimmer D.W., Duffy J.F., Klerman E.B. et al.: Human circadian pacemaker is sensitive to light throughout subjective day without evidence of transients. Am. J. Physiol. Regulatory Integrative Comp. Physiol. V273 (1997) P:R1800-R1809.

[11] Rosenthal N.E., Kasper S.F.: Licht-Therapie. Heyne Ratgeber Nr. 08/5150, 2. Auflage (1998).

[12] Human Centric Lighting: By Stan Walerczyk, CLEP, LC, Principal, Lighting Wizards http://humancentriclighting.com/wp-content/uploads/2012/07/Stan-Article-SSL1.pdf (2015) (Abgerufen am 30.06.2015, 14:00)

[13] Licht.wissen19: Wirkung des Lichts auf den Menschen http://www.licht.de/fileadmin/Publikationen_Downloads/1403_lw19_Wirkung_auf_Mensch_web.pdf (2014) (Abgerufen am 30.06.2015, 14:00)

[14] Bieske K., Vandahl C., Schierz Ch.: Projekt "Licht und Gesundheit" - Feldstudie in Industriebetrieben https://www.tu-ilmenau.de/fileadmin/public/lichttechnik/Publikationen/2011/Bericht_Licht_und_Gesundheit_-_Feldstudie_in_Industriebetrie.pdf (2011) (Abgerufen am 30.06.2015, 14:00)

Institut für Optische Systeme
Hochschule Konstanz
Brauneggerstr. 55
78462 Konstanz
www.ios.htwg-konstanz.de